



HAL
open science

Multiple crust reworking in the French Armorican Variscan belt: implication for the genesis of uranium-fertile leucogranites

Christophe Ballouard, Marc Poujol, Armin Zeh

► **To cite this version:**

Christophe Ballouard, Marc Poujol, Armin Zeh. Multiple crust reworking in the French Armorican Variscan belt: implication for the genesis of uranium-fertile leucogranites. *International Journal of Earth Sciences*, 2018, 107 (7), pp.2317-2336. 10.1007/s00531-018-1600-3 . insu-01717290

HAL Id: insu-01717290

<https://insu.hal.science/insu-01717290>

Submitted on 26 Feb 2018

HAL is a multi-disciplinary open access archive for the deposit and dissemination of scientific research documents, whether they are published or not. The documents may come from teaching and research institutions in France or abroad, or from public or private research centers.

L'archive ouverte pluridisciplinaire **HAL**, est destinée au dépôt et à la diffusion de documents scientifiques de niveau recherche, publiés ou non, émanant des établissements d'enseignement et de recherche français ou étrangers, des laboratoires publics ou privés.

[Click here to view linked References](#)

Multiple crust reworking in the French Armorican Variscan belt: implication for the genesis of uranium-fertile leucogranites

1 **C. Ballouard^{a,b,*}, M. Poujol^b, A. Zeh^c**

2 ^aDepartment of Geology, University of Johannesburg, PO Box 254, Auckland Park 2006,
3 South Africa

4 ^b Univ Rennes, CNRS, Géosciences Rennes - UMR 6118, F-35000 Rennes, France

5 ^c Institute of Applied Geosciences – Karlsruhe Institute of Technology (KIT), Campus South,
6 Mineralogy and Petrology, Adenauerring 20b, 50.4, D-76131 Karlsruhe, Germany

7 *** Correspondence:**

8 christopheballouard@hotmail.fr, christopheb@uj.ac.za, +27648303568

9 **Keywords: peraluminous granites, zircon U-Pb dating, Hf-Nd isotope analyses, Variscan**
10 **orogeny, uranium metallogenesis**

11 **Abstract**

12 Muscovite peraluminous granites (MPGs) form by partial melting of the continental crust and
13 can be related to metalliferous deposits such as tin, tungsten and uranium (U). Metal enrichment
14 in MPGs commonly results from fractional crystallization, but the metal contents of the source
15 play a major role for their fertility. Between ca. 320 and 300 Ma (Late Carboniferous), the
16 French Armorican Variscan belt was intruded by numerous U-fertile MPGs that contain
17 inherited zircon grains with a wide range of ages from Archean-to-Carboniferous. U-Pb and Hf
18 isotopic data of zircon grains from Brioverian-to-Carboniferous sediments, Cambrian-to-Early
19 Carboniferous granitoids and Late Carboniferous MPGs indicate that the crust of the Armorican

20 Massif is made up by detritus mainly derived from the West African craton (3500-1600 Ma;
21 $T_{DM} = 3.8-2.3$ Ga), Grenvillian belt (1200-900 Ma; $T_{DM} = 2.7-1.2$ Ga) and Avalonian-Cadomian
22 belt (800-550 Ma; $T_{DM} = 2.5-0.8$ Ga), and that the crust was affected by magmatic events at
23 510-470 Ma ($T_{DM} = 1.6-0.6$ Ga), 410-330 Ma ($T_{DM} = 1.6-1$ Ga) and 320-300 Ma. Furthermore,
24 they reveal that the Late Carboniferous MPG's were mainly formed by partial melting of
25 Brioverian sediments with Cambro-Ordovician and Devonian-Carboniferous granitoids, which
26 are all genetically linked with each other and characterized by $Th/U < 4$. The new data suggest
27 that the U-fertile MPG's result from multiple reworking of U-rich Brioverian sediments,
28 deposited ca. 550 Ma ago on the northern margin of Gondwana, and partially molten during
29 several Paleozoic events, causing a successive increase in U content in the middle-upper crust.

30 **Introduction**

31 In late orogenic setting, the partial melting of the crust during extensional and/or
32 transcurrent tectonic regimes commonly lead to the emplacement of peraluminous granitoids
33 (e.g. Barbarin 1999) including cordierite bearing peraluminous granites (CPGs), muscovite
34 bearing peraluminous granites (MPGs; Barbarin 1996, 1999) and related LCT (lithium-cesium-
35 tantalum) pegmatites (Černý and Ercit 2005). Peraluminous granites and pegmatites are
36 generally considered to form by the partial melting of sedimentary rocks at lower or
37 intermediate crustal levels (e.g. Bernard-Griffiths et al. 1985; Le Fort et al. 1987; Vielzeuf and
38 Holloway 1988; Patiño-Douce and Johnston 1991; Montel and Vielzeuf 1997; Patiño-Douce
39 1999; Shaw et al. 2016) but highly peraluminous melts can also be produced through the partial
40 melting of mica rich igneous rocks (e.g. Turpin et al. 1990; Castro et al. 1999; Villaseca et al.
41 2012; García-Arias et al. 2015; Gao et al. 2016; Laurent et al. 2017; López-Moro et al. 2017).
42 MPG's and related pegmatites can be associated with various metalliferous deposits such as tin
43 (Sn), tungsten (W), uranium (U), lithium (Li) and tantalum (Ta). The genesis of these deposits
44 relates significantly to fractional crystallization and hydrothermalism but the pre-concentration

45 of these lithophile elements in the source region submitted to partial melting is a necessary
46 requirement for the genesis of peraluminous granites and pegmatites associated with
47 economically significant metal deposits.

48 Recent studies (Romer and Kroner 2015, 2016) suggested that the formation of granites
49 associated with Sn-W deposits and LCT pegmatites may result from weathering-related rare
50 element enrichment in sediments prior to partial melting. Epicontinental black shales deposited
51 after major glaciation events also have the capacity to trap a large amount of U (Cuney 2010)
52 and their partial melting can lead to the formation of U rich melts. Emplacement of igneous
53 rocks formed by the partial melting of an enriched lithospheric mantle can also result in the
54 enrichment of incompatible element in the continental crust (Cuney 2010). Furthermore, crustal
55 reworking can achieve significant metal enrichment at the scale of the lower, middle and upper
56 crust. During granulite-facies metamorphism, dehydration of the lower crust can lead to the
57 production of fluids enriched in F, large ion lithophile elements and rare metals. These fluids,
58 preferentially channeled along regional shear zones, may enhance the partial melting of the
59 middle crust resulting in the formation of magmas enriched in rare metals and U (Cuney and
60 Barbey 2014). A comparable model was proposed by Eglinger et al. (2016) in the Pan African
61 Lufilian belt where a crustal-scale Ca-Na metasomatism has leached U from the basement, and
62 transported and redistribute it into supracrustal rocks along the brittle-ductile transition. Finally,
63 crustal-derived magmatism can also induce significant metal mobility at the scale of the crust.
64 Such process is well recorded in the uraniferous Mesoproterozoic western Namaqua province
65 (South Africa) where voluminous granitic magmatism, recorded for a period of about 200 Ma,
66 led to progressive U enrichment of the lower-middle crust (e.g. Andreoli et al. 2006).

67 In the European Variscan belt (EVB), a large proportion of the hydrothermal U deposits are
68 spatially associated with uraninite bearing low-Ca Late Carboniferous MPGs (e.g. Cathelineau
69 et al. 1990; Cuney et al. 1990; Tischendorf and Förster 1994; Ballouard et al. 2017a, in press)

70 (Fig. 1) and in the Armorican Massif (French part of the EVB) 20.000 t of U (20 % of the
71 French production; UDEPO database: <https://infcis.iaea.org>) were extracted from the deposits
72 spatially associated with the syntectonic MPGs (leucogranites) emplaced in the southern part
73 of the massif (Fig. 2). Overall, most of the MPGs emplaced along the south Armorican shear
74 zone (SASZ), a lithospheric scale strike-slip fault (e.g. Jégouzo 1980; Gumiaux et al. 2004a, b;
75 Gapais et al. 2015), appear to be U-fertile, either because they are the source for several
76 economically significant U deposits, such as the Mortagne (Cathelineau 1982) and Pontivy
77 (Marcoux 1982; Ballouard et al., in press) MPGs or because they liberated an important amount
78 of U during post-magmatic hydrothermal alteration, such as the Questembert MPG (Tartèse et
79 al. 2013). In contrast, MPGs that were emplaced in extensional setting to the south of the SASZ
80 (Gapais et al. 2015), are barren. The only exception is the U-fertile Guérande MPG, which is
81 spatially associated with U deposits (Cathelineau 1981; Ballouard et al. 2017a). The distribution
82 of the U-rich MPGs in the Armorican Massif fits widely the distribution of the so-called high
83 heat production and flow belt (HHPFB; Fig. 2) defined by Jolivet et al. (1989) and Vignerresse
84 et al. (1989). This belt shows a NW-SE orientation, is ca. 50 km wide, and characterized by an
85 elevated heat flux. Granites in this belt have heat production values more than twice the values
86 of the surrounding geological formations (Jolivet et al. 1989; Vignerresse et al. 1989).
87 Vignerresse et al. (1989) therefore suggested that the HHPFB reflects the presence of an upper
88 to intermediate continental crust enriched in radioactive elements and that partial melting of
89 this crust caused the formation of U-fertile MPGs.

90 Recent studies focused mainly on the detailed deciphering of intramagmatic and
91 hydrothermal processes leading to the genesis of the U deposits associated with the Guérande
92 and Pontivy MPGs (Ballouard et al. 2015a, 2017a, 2017b, in press). However, the more global
93 reasons behind the U-fertility of the MPGs in the Armorican Massif, and particularly the role
94 of their source(s), remain unclear. To place new constraints on this open issue new sets of data

95 are presented in this study, comprising whole rock trace elements and Nd-Sr isotopic analyses,
96 U-Pb ages and Hf isotopic data of inherited zircon grains from Late Carboniferous MPGs,
97 detrital zircon from Brioverian to Carboniferous sedimentary rocks and zircon crystals from
98 pre-Late Carboniferous igneous rocks surrounding the MPGs. Finally, the implication of the
99 new data sets for the genesis of U-fertile MPGs is discussed.

100 **Geological context**

101 The Armorican Massif belongs to the European Variscan Belt (EVB), a Paleozoic orogenic
102 belt that extends from Western (Iberian Massif) to Central Europe (Bohemian Massif) and
103 results from the convergence of the Gondwana and Avalonia continents (Fig. 1;) (Ballèvre et
104 al. 2009, 2013, 2014; Kroner and Romer 2013). The oldest rocks from the European Variscan
105 belts are the Icartian orthogneisses that outcrop sporadically to the north of the Armorican
106 Massif (Vidal et al. 1981). These, ca. 2 Ga old metagranitoids, are the witnesses of a
107 Paleoproterozoic continental crust (Samson and D'lemos 1998). The Neoproterozoic-Cambrian
108 Cadomian orogeny represents the main Pre-Variscan orogenic event (Linnemann et al. 2008,
109 2014). Strong Cadomian imprints are preserved in the Saxo-Thuringian domains of the
110 Bohemian and Iberian Massifs, and the main type locality is the northern part of the Armorican
111 Massif (Figs. 1 and 2). The Cadomian-Avalonian orogen is the result of the succession of
112 variable geodynamic events occurring along the northern margin of the West African craton
113 (Gondwana). These events include the formation of a continental magmatic arc from ca. 750 to
114 570 Ma, back-arc basin closure followed by arc-continent collision from ca. 570 to 540 Ma and
115 major granitoid magmatism at ca. 540 Ma (Linnemann et al. 2008, 2014, Koglin et al. 2018).
116 During the Cambro-Ordovician (ca. 510 – 470 Ma), a widespread extension event, leading to
117 the separation of continental micro-blocks (Ibero-Armorica) from the northern Gondwana
118 margin, induced an important magmatism related to the emplacement of various granitoids and
119 volcanic rocks (Fig. 1) (Ballèvre et al. 2012, 2013, 2014; Kroner and Romer 2013; Villaseca et

120 al. 2016; Koglin et al. 2018). Subduction of oceanic then continental domains in the EVB
121 occurred until ca. 350-340 Ma and transition from a compressive to an extensive regime
122 occurred at ca. 315-310 Ma (Kroner and Romer 2013; Ballèvre et al. 2014). From Middle
123 Carboniferous to Early Permian (e.g. Romer et al. 2007; Martínez Catalán et al. 2014; Laurent
124 et al. 2017; Ballouard et al. 2017b), the EVB experienced an important magmatism leading to
125 emplacement of crustal-derived MPGs and CPGs as well as hybrid or mantle-derived K-rich
126 K-feldspar porphyritic calc-alkaline (KCGs) and amphibole-rich calc-alkaline (ACGs)
127 granitoids (Barbarin 1999) (Fig. 1). The EVB represents an important metallogenic province
128 for U where vein, episyenite-type, breccia-hosted or shear zone-hosted U deposits occur
129 throughout the belt (Fig. 1). A large proportion of these hydrothermal deposits are spatially
130 associated with Late Carboniferous MPGs and mineralizing events mostly occurred during the
131 Permian from ca. 300 to 260 Ma (e.g. Cathelineau et al. 1990; Cuney et al. 1990; Tischendorf
132 and Förster 1994; Cuney and Kyser 2008; Romer et al. 2010; Ballouard et al. 2017a, in press).

133 The Armorican Massif is separated into three main domains by the north Armorican shear
134 zone (NASZ) and the south Armorican shear zone (SASZ), two dextral crustal to lithospheric-
135 scale strike-slip faults (Fig. 2) (e.g. Gumiaux et al. 2004b). The northern domain is mostly made
136 of Cadomian basement that belonged to the upper crust during Variscan orogeny (Ballèvre et
137 al. 2001; Brun et al. 2001). The central domain is dominantly composed of Brioverian
138 (Neoproterozoic-Cambrian) to Lower Carboniferous sediments that were mostly deformed
139 under greenschist facies conditions during strike-slip deformation (Gumiaux et al. 2004a).
140 Brioverian sediments in this domain constitute a more than 1000 m thick monotonous and
141 immature detrital succession of wacke-type sandstones (Dabard et al. 1996). The Ordovician to
142 Lower Carboniferous sediments form a heterogeneous mostly siliciclastic succession with a
143 thickness above 3500 m. Carbonates mostly occur in Devonian sediments whereas black shales
144 are characteristic of the Silurian and the Upper Devonian (Pelhate 1994; Vidal et al. 2001). The

145 southern domain, that belongs to the internal part of the Variscan belt, is characterized by an
146 intense deformation and by the presence of high grade metamorphic rocks (e.g. Gapais et al.
147 2015). Three tectono-metamorphic units can be distinguished in this domain and comprise from
148 top to bottom: (i) HP-LT rocks, composed of Ordovician acid metavolcanic rocks (Ballèvre et
149 al. 2012) and blueschists subducted and exhumed between ca. 370 and 350 Ma (e.g. Bosse et
150 al. 2005), (ii) micaschists, and (iii) migmatite-bearing units (Fig. 2). Migmatites, mostly formed
151 by partial melting of pre-Carboniferous sediments and Early Paleozoic orthogneisses and
152 recorded peak P-T condition of 0.8 GPa, 750-850 °C (Jones and Brown 1990; Augier et al.
153 2015).

154 Magmatism in the Armorican Massif occurred during four main periods. During the
155 Cadomian period from ca. 750 to 580 Ma, the northern domain was affected by acid and mafic
156 arc magmatism followed by voluminous granitoid plutonism at ca. 540 Ma (Ballèvre et al. 2001,
157 2013). In the Early Ordovician times (ca. 490 – 470 Ma), intracontinental rifting was
158 responsible for the emplacement of tholeiitic mafic magmas and voluminous acid metavolcanics
159 (Vendée porphyroids) in the southern domain (Ballèvre et al. 2012), whereas Late Cambrian-
160 Early Ordovician granitoids intruded the whole massif (Fig. 2). The Devonian-Early
161 Carboniferous period is marked by the emplacement of gabbros and various granitoids
162 (Marcoux et al. 2009; Capdevila 2010) (Fig. 2) as well as by the development of an extensive
163 network of mafic dikes at ca. 360 Ma (Pochon et al. 2016). This period is related to Early
164 Variscan subduction and initial collision. During the Late Carboniferous (from ca. 320 to 300
165 Ma), dextral wrenching of the central domain and crustal extension in the southern domain, led
166 to the exhumation of migmatitic core complex (Gapais et al. 2015), coeval with the
167 emplacement of three main types of granitoids (Fig. 2).

168 (1) MPGs: they were mostly emplaced either along extensional deformation zone in the
169 internal domain of the Armorican Variscan belt, such as the Quiberon (Gapais et al. 2015) and

170 Guérande (309.7 ± 1.3 Ma: Ballouard et al. 2015a) MPGs, or along the SASZ such as the
171 Questembert (316.1 ± 2.9 Ma: Tartèse et al. 2011b), Lizio (316.4 ± 5.6 Ma: Tartèse et al. 2011a)
172 and Pontivy (316.7 ± 2.5 Ma: Ballouard et al. 2017b) MPGs. Some of them were also emplaced
173 to the north of the SASZ such as the Langonnet (304.7 ± 2.7 Ma: Ballouard et al. 2017b),
174 Huelgoat (314.0 ± 2.8 Ma: Ballouard 2016) and Saint-Renan MPGs (316.0 ± 2.0 Ma: Le Gall
175 et al. 2014). Previous isotopic studies (Bernard-Griffiths et al. 1985; Euzen 1993; Tartèse and
176 Boulvais 2010; Ballouard et al. 2015a, 2017a, 2017b) revealed that these MPGs are
177 characterized by high $\delta^{18}\text{O}$ ratios (> 11), sub-chondritic to chondritic $\epsilon\text{Nd}(\text{T})$ and elevated initial
178 $^{87}\text{Sr}/^{86}\text{Sr}$ (> 0.705) values in agreement with a crustal origin.

179 (2) CPGs: the Rostrenen (Euzen 1993; Ballouard et al. 2017b) and Huelgoat (Georget 1986)
180 CPGs were emplaced at 315.5 ± 2.0 Ma (Ballouard et al. 2017b) and 314.8 ± 2.0 Ma (Ballouard
181 2016), respectively. These granites were emplaced synchronously with small stocks of mantle-
182 derived mafic to intermediate igneous rocks.

183 (3) KCGs: these metaluminous biotite \pm hornblende granitoids consist of a magnesio-
184 potassic (Mg-K) and ferro-potassic (Fe-K) suite emplaced between 325 and 300 Ma and
185 associated with mantle-derived mafic to intermediate rocks (Peucat et al. 1984; Capdevila,
186 2010; Caroff et al. 2015; Ballouard et al. 2015b).

187 At a global scale, crustal partial melting to the south of the SASZ, during the Late
188 Carboniferous, was triggered by lithospheric thinning during late orogenic extension. In
189 contrast, to the north of the SASZ, partial melting of the crust and of a lithospheric mantle,
190 metasomatized during previous subduction events, were likely induced by asthenosphere
191 upwelling during diffuse strike-slip deformation of the central domain and subsequent slab-
192 tearing (Ballouard et al. 2017b).

193 In the Armorican Massif, U was mostly mined in the district of Mortagne, Pontivy and
194 Guérande. In the Guérande and Pontivy districts, the MPGs were the main source for the U
195 mineralization found in the intra to perigranitic vein and episyenite type hydrothermal deposits.
196 Leaching of magmatic U oxides from the MPGs was promoted by the infiltration at depth of
197 oxidized surface-derived hydrothermal fluids (Ballouard et al. 2017a, in press). U-Pb dating of
198 U oxides from the Guérande, Pontivy and Mortagne district deposits reveal several mineralizing
199 events that occurred by pulse from ca. 300 to 260 Ma (Cathelineau et al. 1990; Ballouard et al.
200 2017a, in press).

201 **Samples and methods**

202 A description and the GPS coordinates of Late Carboniferous MPGs, sedimentary rocks,
203 and Cambro-Ordovician granitoid samples selected for whole-rock major and trace element
204 analyses as well as zircon U-Pb and Hf isotope analyses are provided in Table 1 and
205 Supplementary file 1.

206 MPGs selected for U-Pb (and Hf) isotope analyses on inherited zircon grains include the U
207 mineralized Guérande and Pontivy MPGs as well as the Questembert, Lizio, Langonnet and
208 Hulgoats MPGs that are not spatially associated with U deposits (Fig. 2). Most sandstone or
209 siltstone samples (Brioverian to Devonian) were collected in the region of Crozon in the western
210 edge of the central Armorican domain (Fig. 2). In addition, a Lower Carboniferous (this study)
211 and Devonian sandstone (Ducassou et al. 2014) were sampled in the Châteaulin basin (western
212 part of the central domain, Fig. 2) and the Chalonnnes region (eastern part of the central domain,
213 Fig. 2), respectively. One metagranite (sample PLG-1), two metatonalites (samples PLG-2 and
214 PLG-4) and one undeformed granite (sample PLG-3) from the Lower Paleozoic Plouguenast
215 orthogneissic complex (central domain, Fig. 2), as well as one metatonalite (sample QIMP-1)
216 from Moëlan (southern domain, Fig. 2) were also selected for zircon U-Pb dating.

217 ***Whole rock isotopic, major and trace element analyses***

218 Large samples (5 to 10 kg) were crushed in the Geosciences Rennes Laboratory using agate
219 mortars. Chemical analyses were performed by the Service d'Analyse des Roches et des
220 Minéraux (SARM; CRPG-CNRS, Nancy, France) using a ICP-AES for the major elements and
221 a ICP-MS for the trace elements following the techniques described in Carignan et al. (2001).
222 The results of the analyses are provided in Supplementary file 2. Whole rock Sr and Sm-Nd
223 isotope analyses were performed at Geosciences Rennes, on two samples from the Guérande
224 MPG (muscovite-tourmaline coarse grained facies, see Ballouard et al. 2015a) and one Lower
225 Carboniferous sandstone sample from the Châteaulin Basin. The methodology and analytical
226 conditions are described in Ballouard et al. (2017b) and the results of the isotope analyses are
227 provided in Supplementary file 3.

228 ***Zircon U-Pb and Hf isotope analyses***

229 A classical mineral separation procedure was applied to concentrate zircon grains using the
230 facilities available at Geosciences Rennes (Ballouard et al. 2015a). Zircon grains were imaged
231 by cathodoluminescence (CL) using a Reliotron CL system equipped with a digital color
232 camera available at the Geosciences Rennes laboratory.

233 U-Pb dating of zircon was performed by in-situ laser ablation inductively coupled plasma
234 mass spectrometry (LA-ICP-MS) using a ESI NWR193UC Excimer laser coupled to a
235 quadrupole Agilent 7700 x ICP-MS equipped with a dual pumping system to enhance
236 sensibility. The methodology and analytical protocol used to perform the analyses can be found
237 in Ballouard et al. (2015a) and Supplementary file 4. The analyses with a degree of concordance
238 between 90 and 110% are provided in Supplementary file 5 with errors listed at 1σ . Histograms
239 (50 Ma bins) and Kernel density estimates (KDE, 25 Ma bands) of the zircon U-Pb dates were
240 realized using the DensityPlotter software (Vermeesch 2012). $^{206}\text{Pb}/^{238}\text{U}$ dates were used for

241 zircon with a $^{207}\text{Pb}/^{206}\text{Pb}$ date < 1.0 Ga whereas $^{207}\text{Pb}/^{206}\text{Pb}$ dates were used for zircon with a
242 $^{207}\text{Pb}/^{206}\text{Pb}$ date > 1.0 Ga.

243 Hafnium (Hf) isotope analyses were performed at Goethe-University Frankfurt using a
244 Thermo-Finnigan NEPTUNE multicollector ICP-MS coupled to a Resolution M-50
245 (Resonetics) 193 nm ArF Excimer laser (ComPexPro 102F, Coherent), using the procedure
246 outlined in detail in Gerdes and Zeh (2006, 2009) and summarized in Supplementary file 4. The
247 epsilon Hf values [$\epsilon\text{Hf}(t)$] were calculated using the chondritic uniform reservoir (CHUR) as
248 recommended by Bouvier et al. (2008; $^{176}\text{Lu}/^{177}\text{Hf} = 0.0336$ and $^{176}\text{Hf}/^{177}\text{Hf} = 0.282785$) and a
249 decay constant of $1.867 \times 10^{-11} \text{ yr}^{-1}$ (Scherer et al. 2001; Söderlund et al. 2004). The initial
250 $^{176}\text{Hf}/^{177}\text{Hf}_t$, $\epsilon\text{Hf}(t)$ values and hafnium model ages (T_{DM}) (for zircon grains with a degree of
251 concordance between 90 and 110%) were calculated using $^{206}\text{Pb}/^{238}\text{U}$ ages for zircon with
252 $^{206}\text{Pb}/^{207}\text{Pb}$ ages < 1.0 Ga and $^{206}\text{Pb}/^{207}\text{Pb}$ ages for zircon with $^{206}\text{Pb}/^{207}\text{Pb}$ ages > 1.0 Ga. The
253 result of analyses and additional information are provided in Supplementary file 6.

254 **Results**

255 *Geochemical features and U-Th distribution*

256 All investigated Late Carboniferous MPGs of the Armorican Massif are highly
257 peraluminous and characterized by A/CNK [$\text{Al}_2\text{O}_3 / (\text{CaO} + \text{Na}_2\text{O} + \text{K}_2\text{O})$, molar proportions]
258 values > 1.1 (Fig. 3). However, the Huelgoat MPG plot on a different trend than the others
259 MPGs, with relatively higher A/NK values at low A/CNK ratio, reflecting a higher CaO
260 content. In Figure 4, these MPGs are mostly characterized by low and highly variable whole-
261 rock Th/U ratio mostly from ~0.1 to 2, as well as variable U content from 1 to 27 ppm.

262 The whole-rock composition of silicoclastic sediments and peraluminous igneous rocks
263 representing potential source for the Late Carboniferous MPGs were also reported in the U
264 versus Th diagram (Fig. 4). The U contents of the Brioverian and Paleozoic sediments

265 (Ordovician to Devonian) range between ~1 and 7 ppm. However, the Paleozoic sediments
266 generally show much higher Th/U ratios (between ~4 and 7), i.e., above the average value of
267 the upper continental crust (UCC ~ 4), compared to most Brioverian sediments (Th/U ratio
268 mostly between ~2 and 4). Most Ordovician (meta)volcanics (Lower Paleozoic) are
269 characterized by U contents between ~1 and 7 ppm and variable Th/U ratios between ~2 and
270 20 whereas Cambro–Ordovician (Lower Paleozoic) and Early Carboniferous (Pertre MPG)
271 granitoids show more variable U contents between ~2 and 40 ppm and are generally
272 characterized by relatively low but variable Th/U ratios ranging from ~0.5 to 4.

273 *Whole-rock Sr-Nd isotope data*

274 Most MPGs are characterized by elevated initial $^{87}\text{Sr}/^{86}\text{Sr}$ [I_{Sr} (315 Ma)] ratios ranging from
275 0.706 (Pontivy MPG) and 0.719 (Guérande MPG) and negative ϵNd (315 Ma) values ($-2.3 >$
276 ϵNd (315 Ma) > -8.0) with two stage Nd model ages (T_{DM}) between 1.2 (Pontivy and Langonnet
277 MPG) and 1.8 Ga (Guérande MPG, Fig. 5). However, two samples from the Pontivy MPG
278 display super-chondritic ϵNd (315 Ma) values (1.2 and 2.2) with relatively low I_{Sr} (0.704 and
279 0.706) ratios and young T_{DM} (1.0 and 0.9 Ga). As noticed by Bernard-Griffiths et al. (1985),
280 the I_{Sr} (315 Ma) and ϵNd (315 Ma) values of MPG increase and decrease, respectively, from
281 north to south with an evolution from the Pontivy–Langonnet-Lizio MPG, Questembert MPG
282 to Guérande MPG (Figs. 2 and 5).

283 *U-Pb dating*

284 *Inherited zircon from MPG*

285 Zircon grains from all investigated MPGs of the Armorican Massif are generally euhedral.
286 They commonly show inherited cores surrounded by magmatic rims in CL images (Fig. 6). U-
287 Pb ages obtained on inherited zircon cores or grains from the MPGs are reported in form of
288 histograms and KDE in Figure 7. In general, five ages populations can be distinguished which,

289 however do not occur in all MPGs: (1) an Archean-Mesoproterozoic population at 3500-1400
290 Ma, (2) a Grenvillian population at 1200-900 Ma, (3) a Neoproterozoic population at 900-540
291 Ma, (4) a Cambro-Ordovician population at 540-440 Ma and (5) a Silurian–Lower
292 Carboniferous population at 440-330 Ma (Table 1). All MPG samples are dominated by zircon
293 grains of the populations (3), (4) and (5). A significant amount of population (1) zircon occurs
294 only in the Pontivy MPG (8%), and of population (2) zircon in the Guérande MPG (8%; see
295 Fig. 7 and Table 1).

296 *Detrital zircon from sediments*

297 U-Pb dates obtained on detrital zircon grains from the main sedimentary formations of the
298 Armorican Massif are reported in Figure 8 and summarized in Table 1.

299 Zircon grains from the different sedimentary rocks show an euhedral to rounded shape and
300 appear zoned or homogeneous in CL images (Fig. 6). The detrital grains reflect similar age
301 populations (1 to 5) than the ones obtained from the xenocrysts in the MPGs (Table 1).
302 However, the amount of Archean-to-Mesoproterozoic grains (population 1) is higher in the
303 sediments compared to the MPGs, especially in Silurian and Devonian sediments (Fig. 8 and
304 Table 1). The most significant difference is that some samples contain abundant zircon grains
305 of Grenvillian age (population 2), e.g., the Silurian and Devonian sediments from Crozon (24-
306 32%), whereas they are completely absent or very scarce in the Brioverian sandstone from
307 Crozon (1%) and the Lower Carboniferous sediments from Châteaulin (0%). It is important to
308 note that zircon age spectra similar to those of Silurian and Devonian sediments were obtained
309 for an Ordovician sandstone from Crozon (Matteini et al. 2014). A minor Grenvillian
310 population is also observed in the Devonian sandstone from Chalennes (10%; Fig. 8 and Table
311 1).

312 *Zircon from Cambrian to Lower Carboniferous peraluminous (meta)igneous rocks*

313 Results of U-Pb dating reveal that the (meta)granitoids from Plouguenast and Moëlan (Fig.
314 2) intruded between 504.5 ± 1.8 (PLG-2) and 466.2 ± 3.6 Ma (QIMP-1) – (for details see text
315 and diagrams in Supplementary file 7), and that most of them contain inherited components
316 (Fig. 9a and Table 1). Zircon shapes are euhedral to sub-euhedral, and CL images reveal well-
317 developed grow zonation for most grains (Fig. 6). Xenocrystic zircon crystals in the
318 (meta)granitoids overlap in age with the previously defined populations 1 (4%) and 3 (18%,
319 Table 1). Zircon analyses with apparent Silurian to Devonian ages (7%) are interpreted to result
320 from Pb loss (see Supplementary file 7 for details).

321 The result of zircon U-Pb dating performed by Ballèvre et al. (2012) on acid peraluminous
322 (meta)volcanics from the southern domain (Vendée Porphyroids, Fig. 2) are reported in Figure
323 9b and Table 1. These (meta)volcanics contains Neoproterozoic xenocrysts (6%), belonging to
324 the population 3 defined in the Late Carboniferous MPGs, whereas the Early Paleozoic grains
325 (population 4: 93%) brackets the age of intrusion from 494 ± 4 to 472 ± 4 Ma (Ballèvre et al.
326 2012). These ages are much older than those obtained on zircon grains from the Pertre MPG
327 (Vernhet et al. 2009) in the central domain (Fig. 2) that yield $^{206}\text{Pb}/^{238}\text{U}$ ages between 362 ± 2
328 and 330 ± 4 Ma (population 5, 93 %) with a marked peak at ca. 340 Ma, interpreted to reflect
329 the time of intrusion (Fig. 9c and Table 1) (Vernhet et al. 2009). One Neoproterozoic xenocryst
330 belongs to the population 3 defined in the Late Carboniferous MPGs whereas two zircon grains
331 with apparent ages of 323 ± 3 and 321 ± 4 Ma, respectively, reflect Pb loss (Vernhet et al. 2009).

332 *Hf analyses*

333 The results of Hf isotope analyses on inherited zircon grains from MPGs are reported in a
334 $\epsilon\text{Hf}(t)$ versus age diagram (Fig. 10a). The Hf isotope compositions of inherited zircon grains in
335 all investigated MPGs are similar. The rare Archean-to- Paleoproterozoic grains (2890-1590
336 Ma) show superchondritic to subchondritic compositions ($\epsilon\text{Hf}(t) = 3.9$ to -11.5), whereas

337 Mesoproterozoic-to-Carboniferous xenocrysts (1035-329 Ma) yield mostly superchondritic
338 $\epsilon\text{Hf}(t)$ up to +9.1 (> 60%). Superchondritic xenocrysts are predominant in the Pontivy (-14.3 to
339 +8.3), Lizio (-4 to +8.2) and Langonnet (-10.3 to +8.4) MPGs, and mostly characterized by
340 hafnium model ages (T_{DM}) between 1.6 and 0.9 Ga. In contrast, the Questembert MPG (-12.1
341 to 7) is dominated by subchondritic grains, even though most of them also show T_{DM} between
342 1.6 and 0.9 Ga. Then, zircon grains from the Guérande MPG (-14.2 to 9.1) show a wide and
343 relatively continuous range of $\epsilon\text{Hf}(t)$ from sub- to superchondritic (Fig. 10a). About 70% of
344 zircon are characterized by T_{DM} between 1.6 and 0.9 Ga whereas others show older T_{DM} between
345 1.60 and 2.3 Ga.

346 The $\epsilon\text{Hf}(t)$ values of detrital zircon grains from the Brioverian and Lower Carboniferous
347 sediments shows a remarkable overlap with those of the MPGs (Figs. 10b and 10d): Archean-
348 Mesoproterozoic zircon grains (3080-1430 Ma) show T_{DM} from 3.7 to 2.2 Ga and about 75 %
349 of the Neoproterozoic-Carboniferous grains (851-329 Ma) are characterized by T_{DM} between
350 and 1.6 and 0.9 Ga. In contrast, detrital zircon grains in the Silurian and Devonian sedimentary
351 rocks show significantly different Mesoproterozoic-to-Cambrian $\epsilon\text{Hf}(t)$ spectra characterized
352 by a wide range in $\epsilon\text{Hf}(t)$ at 1200-900 Ma (-38 to +10.8; $T_{\text{DM}} = 3.8-1.2$ Ga), and by about 70 %
353 of subchondritic $\epsilon\text{Hf}(t)$ for ages < 900 Ma (-37 to +8; $T_{\text{DM}} = 3.6-1.1$ Ga; Fig. 10b). This
354 difference is also reflected by the generally much older Hf model ages for the Neoproterozoic-
355 to-Cambrian population, with more than 50 % between 1.6 and 2.5 Ga (Fig. 10b). The Hf
356 isotopic data of the Archean-to-Paleoproterozoic grains (2922-1841 Ma; $T_{\text{DM}} = 3.5-2.5$ Ga) in
357 the Silurian-Devonian sediments overlap with those in the Brioverian-Carboniferous sediments
358 and in the MPGs.

359 The $\epsilon\text{Hf}(t)$ values of magmatic zircon grains from the Cambro-Ordovician metagneous
360 rocks (510-460 Ma) vary from -0.7 to +14.2, corresponding to hafnium model ages between
361 1.4 and 0.6 Ga (Fig. 10c). It is pertinent to note, that these T_{DM} overlap with those obtained

362 from most Neoproterozoic-to Carboniferous xenocrysts in the MPGs (Figs. 10a and 10d).
363 However, there is also an important number of grains showing significantly higher $\epsilon_{\text{Hf}}(t)$, very
364 close to the depleted mantle. Such grains were mostly found in sample PLG-1 from the
365 Plouguenast orthogneissic complex (Fig. 10c).

366 **Discussion**

367 *Pre- to Early Variscan zircon record*

368 Neoproterozoic to Early Cambrian zircon grains (850 – 530 Ma, Fig. 7a) in the Brioverian
369 sediments likely result from magma mixing, which occurred during the formation of the
370 Cadomian-Avalonian belt, an Andean-type cordillera located at the northern margin of
371 Gondwana, e.g. to the north of the Armorican Massif (Fig. 2a), between approximately 800 and
372 540 Ma (e.g. Nance and Murphy 1994; Dabard et al. 1996; Ballèvre et al. 2001; Brun et al.
373 2001; Zeh et al. 2001; Linnemann et al. 2008, 2014; Koglin et al. 2018). This hypothesis is
374 supported by the vertical array in the $\epsilon_{\text{Hf}}(t)$ vs. age diagram (array CA in Figure 10d), reflecting
375 the interaction of crustal melts formed by reworking of Archean-to-Paleoproterozoic crust of
376 the West Africa craton ($\epsilon_{\text{Hf}}(t)$ down to -22), and mantle-derived melts ($\epsilon_{\text{Hf}}(t)$ up to +13). Then,
377 most Archean-to-Mesoproterozoic zircon grains (3080 – 1430 Ma; Fig. 8a) likely originated
378 from the erosion of the West African craton (Fig. 10d), that represented the hinter land of the
379 Cadomian orogeny (e.g. Zeh et al. 2001; Linnemann et al. 2008, 2014), whereas the ca. 2000
380 Ma old Icartian orthogneisses (e.g. Samson and D’Lemos 1998) only represented a minor
381 source (e.g. Dabard et al. 1996).

382 The Silurian and Devonian sediments might result from internal reworking of a very
383 heterogeneous Grenvillian crust (indicated by the vertical array G in Fig. 10d), with minor
384 contribution from the Cadomian-Avalonian crust. The Grenville zircon grains are very likely
385 to be derived from a southern Gondwana-connected source, whereas a northern Baltica

386 provenance can be excluded. Indeed, Grenvillian zircon populations were found in many
387 Paleozoic sediments throughout the EVB, commonly associated with a predominant
388 Neoproterozoic-Cambrian (800-500 Ma), and a subordinate Archean-to-Palaeoproterozoic
389 zircon population (1700-3500 Ma), and with a pronounced age gap between 1.2 and 1.7 Ga
390 (e.g. Zeh et al. 2001; Linnemann et al. 2008, 2014). In fact, these are the same features observed
391 in the Armorican sediments during this study (Fig. 10b). In contrast, zircon grains derived from
392 Baltica, have ages mostly between 1.0 and 1.8 Ga, as it has been demonstrated for Paleozoic
393 (meta)sediments from the Rhenohercynian Domain (Avalonia-Laurussia in Fig. 1), and the
394 Mid-German Crystalline Zone (northwestern edge of the Saxo-Thuringian in Fig. 1) of the
395 eastern EVB (Geisler et al. 2005; Zeh and Gerdes 2010).

396 The overlap in zircon Age-Hf isotopic data suggests that the Cambro-Ordovician
397 (meta)granitoids of the Armorican Massif were predominantly formed by partial melting of
398 Brioverian sediments (Fig. 10d). However, the highly superchondritic $\epsilon\text{Hf}(t)$ (near to depleted
399 mantle) signature of some zircon grains from the granitoids of the Plouguenast orthogneissic
400 complex additionally reveals that new (juvenile) crust was formed at the same time. In this
401 context it is pertinent to note that Cambro-Ordovician juvenile crust formation (in addition to
402 crustal melting) is not restricted to the Armorican Massif (e.g. Bernard-Griffiths et al. 1986;
403 Ballèvre et al. 2012) but has been reported from many other areas throughout the EVB, e.g.,
404 from the NW Iberian Massif (e.g. Arenas et al. 2016), French Massif Central (e.g. Chelle-
405 Michou et al. 2017) and Saxothuringian Domain (e.g. Bankwitz et al. 1994; Höhn et al. 2017),
406 where it is related to the breakup of continental microterranes from the northern Gondwanan
407 margin (e.g. Kroner and Romer 2013). The relatively wide variation in $\epsilon\text{Hf}(t)$ of the Cambro-
408 Ordovician metagneous rocks (array R in Fig. 10d) is ambiguous. It could be explained by
409 heterogeneities of the source (Brioverian sediments), but, more probably, by mixing of juvenile

410 melts (depleted mantle-related) and crustal-derived melts, formed by the partial melting of
411 Brioverian sediments.

412 The Age-Hf-isotopic data furthermore suggest that the Brioverian sediments and the
413 Cadomian-Avalonian basement together with Cambro-Ordovician igneous rocks were the main
414 sources for the detrital zircon grains in the Lower Carboniferous sediments (Fig. 10b).
415 Moreover, a significant addition from zircon grains derived from Early Variscan granitoids
416 emplaced between ~400 and 330 Ma (array EV in Fig. 10d) such as the ca. 340 Ma old Pertre
417 granite (Fig 9c), is revealed by isotopic data. Most 390 to 330 Ma old zircon grains in the Lower
418 Carboniferous sediments are characterized by T_{DM} from 1.2 to 1.6 Ga that overlap with those
419 of Neoproterozoic zircon in the Brioverian sediments (Figs 10b and d), suggesting that these
420 zircon grains crystallized in a crustal-derived granitic magma formed by the partial melting of
421 Brioverian sediments. This hypothesis is in agreement with the presence of a ca. 625 Ma old
422 zircon xenocryst in the Pertre granite (Fig. 9c, Table 1).

423 *Crustal sources of Late Carboniferous MPGs*

424 The highly peraluminous character ($A/CNK > 1.1$, Fig. 3) of the MPGs is in agreement with
425 a crustal origin and suggest that they were produced by the partial melting of mica-rich rocks
426 with a peraluminous composition (e.g. Gao et al. 2016).

427 Whole-rock Nd and Sr isotope analyses indicate a significant difference in composition
428 between the MPGs emplaced to the north of the SASZ (i.e. Pontivy, Langonnet, Lizio) and the
429 Guérande MPG intruded to south of the SASZ (Figs. 2 and 5). The Questembert MPG, which
430 emplaced between the two branches of the SASZ, has an intermediate composition. The
431 negative $\epsilon Nd(315 \text{ Ma})$ values of the Guérande MPG (-7.6 to -9.5) could be explained by the
432 partial melting of Cambro-Ordovician acid (meta)volcanic rocks as well as Ordovician to
433 Devonian sediments from the south Armorican domain, although some samples plot at the

434 lower boundary of the range defined by Brioverian sediments from the central domain (Fig. 5).
435 The $\epsilon\text{Nd}(315 \text{ Ma})$ values of the Questembert MPG (-3.9 to -5.7) overlap with those obtained
436 from the Brioverian sediments from the central domain as well as with Cambro-Ordovician acid
437 (meta)volcanic rocks. Then, the composition of the Pontivy, Langonnet and Lizio MPGs (-2.3
438 to -4.7) is similar to that of Brioverian sediments from the central domain as well as the Cambro-
439 Ordovician (meta)granitoids and (meta)volcanic rocks. The super-chondritic $\epsilon\text{Nd}(315 \text{ Ma})$
440 composition of two Pontivy MPG samples could be explained by the partial melting of Cambro-
441 Ordovician (meta)granitoids. However, the Nd isotopic values on their own are ambiguous, and
442 do not allow a detailed source characterization. Two reasons may be proposed at this stage.
443 First, the MPG melts can be derived from several sources and, second, some sources show a
444 wide range in ϵNd values (Fig. 5), e.g., the Cambro-Ordovician acid (meta)volcanics rocks,
445 which themselves were formed by melting of even older crustal components such as Brioverian
446 sediments (Ballèvre et al. 2012).

447 Combined U-Pb and Hf isotopic data of zircon xenocrysts (2890-329 Ma; Table 1; Figs. 7
448 and 10d) suggest that the Late Carboniferous MPGs were formed by partial melting of a
449 heterogeneous crust mainly consisting of Brioverian sediments, Cambro-Ordovician acid
450 igneous rocks and Devonian to Early Carboniferous granitoids. In contrast, Ordovician to
451 Devonian sedimentary rocks seems to play only a subordinate role during U-fertile MPGs
452 formation for several reasons. First, they contain an important Grenvillian population (1.2-0.9
453 Ma: this study, Matteini et al. 2014) with a wide range in $\epsilon\text{Hf}(t)$ (-38 to 10.8), which is barely
454 seen in the xenocrysts from the MPGs (Fig. 10d). The only exceptions are four grains (8%) in
455 the Guérande MPG and one grain in the Lizio (3%) and Pontivy (1%) MPGs, respectively
456 (Table 1, Figs 7). Second, the Silurian and Devonian sediments contain a pronounced Archean
457 to Mesoproterozoic population (3.5-1.4 Ga; 23-36%) which is not observed in the MPGs (<
458 10%, Table 1). Third, detrital zircon grains from Silurian to Devonian sediments with ages <

459 0.9 Ga mostly show subchondritic $\epsilon\text{Hf}(t)$ values (ca. 70%), corresponding to Hf model ages of
460 2.5 to 1.6 Ga, which are much older than those of most MPGs (0.9 to 1.6 Ga). On the other
461 hand, a significant number of Neoproterozoic to Carboniferous (750-329 Ma) zircon with old
462 T_{DM} from 1.6 to 2.5 Ga (Fig. 10a) together with some Grenvillian grains (1080-974 Ma; Fig.
463 7f) in the Guerande MPG suggests a minor contribution of Ordovician to Devonian sediments
464 in its source, in agreement with its high sub-chondritic ϵNd composition (Fig. 5). Moreover, the
465 contribution of Lower Carboniferous sediments in the source of all MPGs is unlikely and
466 difficult to explain structurally. Indeed, the central domain that was mainly deformed under
467 strike-slip deformation regime during the Carboniferous was poorly thickened during the
468 Variscan orogeny (Gumiaux et al. 2004a; Gapais et al. 2015) and the burying, and subsequent
469 partial melting, of Lower Carboniferous sediments probably never occurred in the central
470 domain. Then, it is unlikely that important partial melting of the Lower Carboniferous
471 sediments occurred in the region without partial melting of Ordovician to Devonian sediments
472 that are structurally below. Alternatively, the partial melting of the Devonian to Early
473 Carboniferous granitoids such as the 391-385 Ma old peraluminous Plounévez-Lochrist
474 orthogneiss (Marcoux et al. 2009) (Fig. 2) can explain the younger range of inheritance
475 observed in all the MPGs (population 5, Table 1). Finally, metatexites and diatexites derived
476 from pre-Carboniferous sediments and Ordovician orthogneisses are abundant in the southern
477 Armorican domain (e.g. Augier et al. 2015) (Fig. 2). These rocks reached peak P-T conditions
478 of 0.8 GPa, 750-850 °C followed by near isothermal decompression down to 0.4 GPa, 750 °C
479 and melting occurred, during the Late Carboniferous, from water saturated solidus to biotite
480 breakdown conditions (Augier et al. 2015; Jones and Brown, 1990), in agreement with the role
481 of Brioverian sediments and Paleozoic orthogneisses as a major source for the MPGs.

482 *Implication for the U-fertility of MPGs*

483 The results of this study show that the U-fertile Pontivy and Questembert MPGs, and the
484 U-unfertile Lizio, Langonnet and Hulgoat MPGs, all emplaced to the north of the southern
485 branch of the SASZ, result from the melting of the same heterogeneous crust, which consisted
486 of Brioverian sediments, Cambro-Ordovician acid igneous rocks and Devonian-to-
487 Carboniferous granitoids. Similar hafnium model ages furthermore suggest that all these rocks
488 are genetically linked, and result from the successive internal reworking of Brioverian
489 sediments (Fig. 10d). Age-Hf isotopic data also suggest that the U-fertile Guérande MPG,
490 emplaced to the south of the SASZ, result from the partial melting of a similar crust with only
491 a minor contribution from Ordovician to Devonian sediments.

492 Thus, fertility or non-fertility of the Late Carboniferous MPGs from the Armorican Massif
493 is obviously controlled primarily by differences during the reworking process, comprising local
494 variations of source rocks (sediment vs. orthogneiss), degree of melting and fractionation, and
495 the melting history itself (unique or multiple), as well as hydrothermal processes during and
496 after each magmatic cycle. The complex interplay of all these processes has been demonstrated
497 by recent studies suggesting that the Lizio and Questembert MPGs represent “twin”
498 leucogranites but that the Questembert MPG is more differentiated than the Lizio MPG because
499 the former traveled a greater vertical distance in the crust, enhancing crystal segregation from
500 the melts and U enrichment in the residual liquids (Tartese and Boulvais 2010; Tartèse et al.
501 2013).

502 The formation of U rich peraluminous liquid is favored by an elevated U content of its
503 sedimentary and/or igneous sources. However, the proportion of U located outside the lattice
504 of accessory minerals poorly soluble in peraluminous melts, such as zircon and monazite
505 (Watson and Harrison 1983; Montel 1993), has a primordial importance for the genesis of U-
506 fertile MPGs (e.g. Cuney 2014). In the absence of a detailed petrographic study, the whole-rock
507 Th/U ratio can be used as a preliminary indicator of the fertility of a rock for the genesis of U-

508 rich melts during anatexis. High Th/U ratios, above the average value of the upper continental
509 crust (UCC Th/U value = 3.8, Rudnick and Gao 2003), suggest that most U is hosted in Th-
510 bearing, highly refractory, minerals such as monazite (xenotime and zircon), whereas Th/U
511 ratios < 3.8 suggest that a significant amount of U is localized along microcracks or in
512 adsorption on the surfaces of rock forming minerals. In most favorable cases, peraluminous
513 igneous rocks with Th/U < 1 and U contents > ~10 ppm can host U oxides (Peiffert et al. 1996,
514 1994). By taking these points into account, we suggest that the U-fertile MPGs (~0.1 < Th/U <
515 ~2, Fig. 4) of the Armorican Massif were formed by partial melting of peraluminous mica-rich
516 lithologies characterized by Th/U < ~4 and U content > ~2.7 ppm (average UCC values). Such
517 rocks comprise the Brioverian sediments, but also Cambro-Ordovician and Devonian-Early
518 Carboniferous peraluminous igneous rocks (Fig. 4). In contrast, the Ordovician to Devonian
519 sediments and Cambro-Ordovician acid volcanic rocks with Th/U > 4 and U < 2.7 ppm, can be
520 considered as less fertile. Our new data also suggest that U-fertility of a crust increases if one-
521 and-the same (peraluminous) crust is affected by multiple melting events, which obviously
522 occurred in the Armorican Massif during the internal reworking of already U-rich (low Th/U)
523 Brioverian sediments during the Cambro-Ordovician, Devonian-Lower Carboniferous and
524 finally during the Upper Carboniferous, in particular along or close to the crustal to lithospheric
525 scale shear zones. More specifically, multiple crustal reworking can induce progressive U
526 enrichment of some crustal domains (i.e. middle crust) and in late orogenic context, the melting
527 of these domains can lead to the formation of U-fertile granites. These interpretations are in
528 good agreement with the fact that peraluminous orthogneisses of Cambro-Ordovician, and
529 Devonian-Early Carboniferous ages occur in the source regions of nearly all Late Carboniferous
530 MPGs throughout the EVB, comprising the French Massif Central (Turpin et al. 1990; Laurent
531 et al. 2017), the Iberian Massif (e.g. Villaseca et al. 2012 ; López-Moro et al. 2017), and the
532 Bohemian Massif in Germany and the Czech Republic (Tichomirowa et al. 2012), three

533 historical mining provinces for granite-related hydrothermal U deposits (Fig. 1). In this context,
534 it is interesting to note that, the Cambro-Ordovician Saint-Goueno MPG from the Plouguenast
535 orthogneissic complex in the Armorican Massif (Fig. 2) hosts intragranitic U occurrences
536 (Carric et al., 1980), suggesting that it contained magmatic U oxides, and reached U-fertility
537 long before the Variscan orogeny.

538 *Comparison with other uraniumiferous provinces worldwide*

539 In the Armorican Variscan belt, multiple partial melting of the crust is associated with
540 progressive increase of the U-fertility of crustal-derived granitoids with time (Fig. 4). This is
541 revealed by, in general, a progressive decrease of the Th/U ratio from the Brioverian sediments
542 ($\sim 2 < \text{Th/U} < \sim 4$), Cambrian-Early Carboniferous granitoids ($\sim 0.5 < \text{Th/U} < \sim 4$) to Late
543 Carboniferous MPGs ($\sim 0.1 < \text{Th/U} < \sim 2$). To see if this behavior can be generalized to other
544 crustal domains, we report in Figure 11 the evolution of the Th-U contents of granitoids from
545 two major U provinces for comparison, from:

546 (1) the Archean Gabonese craton that surrounds the Paleoproterozoic Franceville basin,
547 well known for hosting U deposits with natural fission reactors such as Oklo.
548 Ultimately, the U from the deposits likely originates from the leaching of U-rich
549 minerals present in the basin, such as monazite, thorite and possibly uraninite,
550 themselves coming from the erosion of the surrounding Archean basement (e.g.
551 Gauthier-Lafaye and Weber 2003). In the basement, granitoid plutonism occurred from
552 2.94 to 2.71 Ga with an evolution from TTG gneiss, grey granitoids, pink granitoids to
553 Neoproterozoic granites and pegmatites (Thiéblemont et al. 2009).

554 (2) the Mesoproterozoic western Namaqualand province, South Africa, representing a
555 granulite- to amphibolite-facies metamorphic terrane characterized by the presence of
556 granites and charnokites highly enriched in U and Th (Andreoli et al. 2006). In the

557 region, crustal-derived granitic magmatism occurred over a period of ca. 200 Ma (Robb
558 et al. 1999).

559 Despite the different degree of enrichment, by one order of magnitude, the U (and Th)
560 contents of the granitoids from both provinces increase progressively and significantly with
561 time. In the Gabonese craton, U increase from ~0.1-0.2 ppm (TTG), ~0.2-1 ppm (grey
562 granitoids) to ~1-4 ppm (pink granites), and in the Namaqualand province, from ~1-10 ppm
563 (Little Namaqualand suite), 3-60 ppm (Early Spektakel suite) to 3-800 ppm (Late Spektakel
564 suite). In the two provinces, fractionation of U over Th, a process that can lead, ultimately, to
565 the crystallization of magmatic uraninite (Cuney, 2014), is only recorded by the youngest
566 granites and pegmatites (Neoproterozoic granites and pegmatites in Fig. 11a and granites of the
567 Late Spektakel suite in Fig. 11b). To summarize, the recycling of the crust by multiple partial
568 melting events seems to be an important mechanism for the concentration of U, the fractionation
569 of U over Th, and finally for the genesis of U-fertile granites.

570 **Conclusion**

571 (1) Age-Hf isotopic data of detrital zircon grains in Brioverian to Carboniferous sediments,
572 magmatic and inherited zircon crystals in Cambrian to Early Carboniferous (meta)igneous
573 rocks, and xenocrysts in the Late Carboniferous MPGs indicate that the crust of the
574 Armorican Massif is made up by detritus derived from three major sources: West African
575 craton (3500-1600 Ma; $T_{DM} = 3.8$ to 2.2 Ga), Grenville belt/domains (1200-900 Ma; T_{DM}
576 = 2.7 to 1.2 Ga), and predominately Avalonian-Cadomian belt (800-550 Ma; $T_{DM} = 2.5$ to
577 0.8 Ga). Moreover, the crust was affected by magmatic events at 510-460 Ma (Cambro-
578 Ordovician; $T_{DM} = 1.6$ to 0.6 Ga), 410-330 Ma (Devonian-Carboniferous; $T_{DM} = 2.1$ to 1.0
579 Ga), and 320-300 Ma (Late Carboniferous).

580 (2) These data also reveal that the Late Carboniferous MPGs (300-320Ma) were mainly formed
581 by partial melting of Brioverian sediments, Cambro-Ordovician igneous rocks and
582 Devonian-Early Carboniferous granitoids, which are all genetically linked with each other,
583 as is indicated by a remarkable overlap in their Hf model ages between 1.6 to 0.8 Ga. In
584 contrast, Ordovician, Silurian and Devonian sediments of the Armorican Massif contain a
585 significant Grenvillian zircon population (~ 30%) with mostly older Hf model ages
586 between 1.6 and 2.5 Ga, which are barely seen in the Late Carboniferous MPGs (Huelgoat,
587 Langonnet, Pontivy, Lizio and Questembert), except for a minor amount in the Guérande
588 MPG (~ 10%).

589 (3) In contrast to Ordovician to Devonian sediments ($\text{Th}/\text{U} > 4$), Brioverian sediments and
590 Cambrian to Early Carboniferous granitoids characterized by $\text{U} > 2.7$ ppm and $\text{Th}/\text{U} < 4$
591 represent an ideal source for the generation of U-fertile MPGs.

592 (4) All data suggests that the U-fertile MPGs of the Armorican Massif result mainly from
593 multiple internal reworking of relatively U-rich Brioverian sediments, which were
594 originally deposited along the northern Gondwanan margin at ca. 550 Ma, and became
595 partially molten during several Paleozoic events, causing a successive increase in U-
596 content by crystal fractionation, and intermediate hydrothermal processes in the middle-
597 upper crust. Similar multiple, internal reworking processes of Neoproterozoic-Cambrian
598 sediments is recorded by rocks from many areas across the EVB hosting economically
599 important U deposits, such as Iberia, French Massif Central and Bohemian Massif.

600 (6) Comparison with other U provinces of different ages worldwide suggest that crustal
601 reworking by multiple partial melting events is a major mechanism for U concentration,
602 fractionation of U over Th, and the genesis of U-fertile granites.

603 **Acknowledgment**

604 This work was supported by the 2012-2013 NEED-CNRS (AREVA-CEA) and 2015-
605 CESSUR-INSU (CNRS) grants attributed to M. Poujol. We are very grateful to M.P. Dabard
606 as well M. Jolivet, R. Tartèse and P. Bessin who helped for the sampling. We also want to
607 thanks Y. Lepagnot and D. Vilbert (Geosciences Rennes) for crushing the samples and realizing
608 whole-rock radiogenic isotope analyses (Sm-Nd and Sr), respectively. Comments from C.
609 Villaseca and A.S. André-Mayer significantly improved the quality of the manuscript. Finally,
610 this study is dedicated to the memory of M.P. Dabard who left us too early.

611 **References**

- 612 Andreoli MAG, Hart RJ, Ashwal LD, Coetzee H (2006) Correlations between U, Th Content
613 and Metamorphic Grade in the Western Namaqualand Belt, South Africa, with implications for
614 radioactive heating of the crust. *J Petrol* 47: 1095–1118
- 615 Augier R, Choulet F, Faure M, Turrillot P (2015) A turning-point in the evolution of the
616 Variscan orogen: the ca. 325 Ma regional partial-melting event of the coastal South Armorican
617 domain (South Brittany and Vendée, France). *Bull Société Géologique Fr* 186: 63–91
- 618 Arenas R, Sánchez Martínez S, Díez Fernández R, Gerdes A, Abati J, Fernández-Suárez J,
619 Andonaegui P, González Cuadra P, López Carmona A, Albert R, Manuel Fuenlabrada J, Rubio
620 Pascual FJ (2016) Allochthonous terranes involved in the Variscan suture of NW Iberia: A
621 review of their origin and tectonothermal evolution. *Earth-Sci Rev* 161: 140–178
- 622 Bailie R, Armstrong R, Reid D (2007) The Bushmanland Group supracrustal succession,
623 Aggeneys, Bushmanland, South Africa: Provenance, age of deposition and metamorphism.
624 *South Afr J Geol* 110: 59–86
- 625 Ballèvre M (2016) Une histoire géologique du Massif armoricain. *Géochronique* 140

626 Ballèvre M, Martínez Catalán JR, López-Carmona A, Pitra P, Abati J, Díez Fernández R,
627 Ducassou C, Arenas R, Bosse V, Castiñeiras P, Fernández-Suárez J, Gómez Barreiro J, Paquette
628 JL, Peucat JJ, Poujol M, Ruffet G, Sánchez Martínez S (2014) Correlation of the nappe stack
629 in the Ibero-Armorican arc across the Bay of Biscay: a joint French– Spanish project. *Geol Soc*
630 *London Spec Publ* 405: 77–113

631 Ballèvre M, Bosse V, Dabard MP, Ducassou C, Fourcade S, Paquette JL, Peucat JJ, Pitra, P
632 (2013) Histoire géologique du Massif armoricain: actualité de la recherche. *Bulletin de la*
633 *Société géologique et minéralogique de Bretagne* 500: 5-96.

634 Ballèvre M, Fourcade S, Capdevila R, Peucat JJ, Cocherie A, Fanning CM (2012)
635 Geochronology and geochemistry of Ordovician felsic volcanism in the Southern Armorican
636 Massif (Variscan belt, France): Implications for the breakup of Gondwana. *Gondwana Res* 21:
637 1019–1036

638 Ballèvre M, Bosse V, Ducassou C, Pitra, P (2009) Palaeozoic history of the Armorican Massif:
639 Models for the tectonic evolution of the suture zones. *Comptes Rendus Geosci* 341: 174–201

640 Ballèvre M, Le Goff E, Hébert R (2001) The tectonothermal evolution of the Cadomian belt of
641 northern Brittany, France: a Neoproterozoic volcanic arc. *Tectonophysics* 331: 19–43

642 Ballouard C (2016) Origine, évolution et exhumation des leucogranites peralumineux de la
643 chaîne hercynienne armoricaine: implication sur la métallogénie de l'uranium. Dissertation,
644 Université de Rennes 1

645 Ballouard C, Poujol M, Mercadier J, Deloule E, Boulvais P, Cuney M, Cathelineau M (in press)
646 Uranium metallogenesis in the peraluminous leucogranites from the Pontivy-Rostrenen
647 magmatic complex (French Armorican Variscan Belt): the result of long term oxidized

648 hydrothermal alteration during strike-slip deformation. *Miner deposita*. DOI : 10.1007/s00126-
649 017-0761-5

650 Ballouard C, Poujol M, Boulvais P, Zeh A (2017b) Crustal recycling and juvenile addition
651 during lithospheric wrenching: The Pontivy-Rostrenen magmatic complex, Armorican Massif
652 (France), Variscan belt. *Gondwana Res* 49: 222–247

653 Ballouard C, Poujol M, Boulvais P, Mercadier J, Tartèse R, Venneman T, Deloule E, Jolivet
654 M, Kéré I, Cathelineau M, Cuney M (2017a) Magmatic and hydrothermal behavior of uranium
655 in syntectonic leucogranites: The uranium mineralization associated with the Hercynian
656 Guérande granite (Armorican Massif, France). *Ore Geol Rev* 80: 309–331

657 Ballouard C, Poujol M, Jolivet M, Boulvais P, Tartese R, Dubois C, Hallot E, Dabard MP,
658 Ruffet G (2015b) Geochronological and thermochronological constraints on the Carboniferous
659 magmatism from the Armorican Massif: from the source to the exhumation. *The Variscan Belt:
660 Correlations and Plate Dynamics, Variscan Conference 2015, Rennes (France), 9–11 June 2015*

661 Ballouard C, Boulvais P, Poujol M, Gapais D, Yamato P, Tartèse R, Cuney M (2015a) Tectonic
662 record, magmatic history and hydrothermal alteration in the Hercynian Guérande leucogranite,
663 Armorican Massif, France. *Lithos* 220–223: 1–22

664 Bankwitz P, Bankwitz E, Kramer W, Pin C (1994) Early Paleozoic bimodal volcanism in the
665 Vesser area, Thuringian Forest, eastern Germany. *Z Geol Paläontol* 1992: 1113-1132

666 Barbarin B (1996) Genesis of the two main types of peraluminous granitoids. *Geology* 24: 295–
667 298

668 Barbarin B (1999) A review of the relationships between granitoid types, their origins and their
669 geodynamic environments. *Lithos* 46: 605–626

670 Béchenec F, Thiéblemont D (2013) Baud 384, Carte géologique de France 1:50 000. BRGM

671 Béchenec F, Hallégouët B, Thiéblemont D (2001) Rosporden 347, Carte Géologique de
672 France 1:50 000. BRGM

673 Béchenec F, Hallégouët B, Thiéblemont D (1999) Quimper 346, Carte Géologique de France
674 1:50 000. BRGM

675 Béchenec F, Guennoc P, Guerrot C, Leuret P, Thiéblemont D (1996) Concarneau 382, Carte
676 Géologique de France 1:50 000. BRGM

677 Bernard-Griffiths J, Carpenter MSN, Peucat JJ, Jahn BM (1986) Geochemical and isotopic
678 characteristics of blueschist facies rocks from the Île de Groix, Armorican Massif (northwest
679 France). *Lithos* 19: 235–253

680 Bernard-Griffiths J, Peucat JJ, Sheppard S, Vidal P (1985) Petrogenesis of Hercynian
681 leucogranites from the southern Armorican Massif: contribution of REE and isotopic (Sr, Nd,
682 Pb and O) geochemical data to the study of source rock characteristics and ages. *Earth Planet
683 Sci Lett* 74: 235–250

684 Bosse V, Féraud G, Ballèvre M, Peucat JJ, Corsini M (2005) Rb–Sr and $^{40}\text{Ar}/^{39}\text{Ar}$ ages in
685 blueschists from the Ile de Groix (Armorican Massif, France): Implications for closure
686 mechanisms in isotopic systems. *Chem Geol* 220: 21–45

687 Bouvier A, Vervoort JD, Patchett PJ (2008) The Lu–Hf and Sm–Nd isotopic composition of
688 CHUR: Constraints from unequilibrated chondrites and implications for the bulk composition
689 of terrestrial planets. *Earth Planet Sci Lett* 273: 48–57

690 Bouton P, Thiéblemont D, Gouin J, Moussavou M (2009) Notice explicative de la Carte
691 géologique de la République du Gabon à 1: 200 000, Feuille Franceville – Boumango, Editions
692 DGMG – Ministères des Mines, du Pétrole, des Hydrocarbures. Libreville

693 Brun JP, Guennoc P, Truffert C, Vairon J (2001) Cadomian tectonics in northern Brittany: a
694 contribution of 3-D crustal-scale modelling. *Tectonophysics* 331: 229–246

695 Capdevila R (2010) Les granites varisques du Massif Armoricain. *Bulletin de la Société*
696 *Géologique et Minéralogique de Bretagne* 7: 1–52

697 Carignan J, Hild P, Mevelle G, Morel J, Yeghicheyan D (2001) Routine Analyses of Trace
698 Elements in Geological Samples using Flow Injection and Low Pressure On-Line Liquid
699 Chromatography Coupled to ICP-MS: A Study of Geochemical Reference Materials BR, DR-
700 N, UB-N, AN-G and GH. *Geostand Newsl* 25: 187–198

701 Carric G, Chantraine J, Dadet P, Flageollet JC, Sagon JP, Talbot H (1980) Montcontour 279,
702 Carte géologique de France 1: 50 000. BRGM

703 Caroff M, Labry C, Le Gall B, Authemayou C, Grosjean DB, Guillong M (2015) Petrogenesis
704 of late-Variscan high-K alkali-calcic granitoids and calc-alkalic lamprophyres: The Aber-
705 Ildut/North-Ouessant complex, Armorican Massif, France. *Lithos* 238: 140–155

706 Castro A, Patiño-Douce AE, Corretgé LG, de la Rosa JD, El-Biad M, El-Hmidi H (1999) Origin
707 of peraluminous granites and granodiorites, Iberian massif, Spain: an experimental test of
708 granite petrogenesis. *Contrib Mineral Petrol* 135: 255–276

709 Cathelineau M (1982) Les gisements d'uranium liés spatialement aux leucogranites sud
710 armoricains et à leur encaissant métamorphique: relations et interactions entre les

711 minéralisations et divers contextes géologiques et structuraux. Sciences de la Terre, Mémoires
712 42. Université de Nancy.

713 Cathelineau M (1981) Les Gisements Uranifères de la Presqu'île Guerandaise (Sud Bretagne);
714 Approche Structurale et Metallogénique. *Miner Deposita* 16: 227–240

715 Cathelineau M, Boiron MC, Holliger P, Poty B (1990) Metallogenesis of the French part of the
716 Variscan orogen. Part II: Time-space relationships between U, Au and Sn-W ore deposition and
717 geodynamic events - mineralogical and U-Pb data. *Tectonophysics* 177: 59–79

718 Černý P, Ercit TS (2005) The Classification of Granitic Pegmatites Revisited. *Can Mineral* 43:
719 2005–2026

720 Cháb J, Stráník Z, Eliáš M (2007) Geologická mapa České republiky 1: 500 000. Česká
721 geologická služba, Praha, Czech Republic

722 Chantraine J, Autran J, Cavalier C (2003) Carte géologique de la France 1: 1 000 000, 6ème
723 édition révisée. BRGM

724 Chelle-Michou C, Laurent O, Moyen JF, Block S, Paquette JL, Couzinié S, Gardien V,
725 Vanderhaeghe O, Villaros A, Zeh A (2017) Pre-Cadomian to late-Variscan odyssey of the
726 eastern Massif Central, France: formation of the West European crust in a nutshell. *Gondwana*
727 *Res* 46: 170-190

728 Civis Llovera J (2015) Mapas geológicos de España y Portugal 1:1 000 000. IGME: Instituto
729 Geológico y Minero de España

730 Clifford TN, Barton ES, Stern RA, Duchesne JC (2004) U–Pb Zircon Calendar for Namaquan
731 (Grenville) Crustal Events in the Granulite-facies Terrane of the O'okiep Copper District of
732 South Africa. *J Petrol* 45: 669–691

733 Cuney M (2014) Felsic magmatism and uranium deposits. *B Soc Geol Fr* 185: 75–92

734 Cuney M (2010) Evolution of uranium fractionation processes through time: driving the secular
735 variation of uranium deposit types. *Econ Geol* 105: 553–569

736 Cuney M, Barbey P (2014) Uranium, rare metals, and granulite-facies metamorphism. *Geosci*
737 *Front* 5: 729–745

738 Cuney M, Kyser T K (2008) Recent and not-so-recent developments in uranium deposits and
739 implications for exploration. Mineralogical Association of Canada, Short Course Series 39

740 Cuney M, Friedrich M, Blumenfeld P, Bourguignon A, Boiron MC, Vignerresse JL, Poty B
741 (1990) Metallogensis in the French part of the Variscan orogen. Part I: U preconcentrations in
742 pre-Variscan and Variscan formations - a comparison with Sn, W and Au. *Tectonophysics* 177:
743 39–57

744 Dabard MP, Peucat JJ (2001) Les métasédiments de Bretagne sud. Rapport BRGM

745 Dabard MP (1997) Les Formations à cherts carbonés (phtanites) de la chaîne cadomienne;
746 genèse et signification géodynamique; exemple du segment Armoricaïn. Documents du BRGM
747 267

748 Dabard MP, Loi A, Peucat JJ (1996) Zircon typology combined with Sm-Nd whole-rock
749 isotope analysis to study Brioverian sediments from the Armorican Massif. *Sediment Geol* 101:
750 243–260

751 Duchesne JC, Auwera JV, Liégeois JP, Barton ES, Clifford TN (2007) Geochemical constraints
752 of the petrogenesis of the O’okiep Koperberg Suite and granitic plutons in Namaqualand, South
753 Africa: A crustal source in Namaquan (Grenville) times. *Precambrian Res* 153: 116–142

754 Ducassou C, Poujol M, Ruffet G, Bruguier O, Ballèvre M (2014) Relief variation and erosion
755 of the Variscan belt: detrital geochronology of the Palaeozoic sediments from the Mauges Unit
756 (Armorican Massif, France). *Geol Soc Lond Spec Publ* 405: 137–167

757 Eglinger A, Vanderhaeghe O, André-Mayer AS, Goncalves P, Zeh A, Durand C, Deloule E
758 (2016) Tectono-metamorphic evolution of the internal zone of the Pan-African Lufilian
759 orogenic belt (Zambia): Implications for crustal reworking and syn-orogenic uranium
760 mineralizations. *Lithos* 240–243: 167–188

761 Euzen T (1993) Pétrogenèse des granites de collision post-épaississement. Le cas des granites
762 crustaux et mantelliques du complexe de Pontivy-Rostrenen (Massif Armoricain, France).
763 *Mémoires Géosciences Rennes* 51

764 Fusán O, Kodým O, Matějka A et al. (1967) Geological map of Czechoslovakia 1:500 000.
765 Czech Geological Survey, Praha

766 Gao P, Zheng Y, Zhao Z (2016) Experimental melts from crustal rocks: A lithochemical
767 constraint on granite petrogenesis. *Lithos* 266: 133–157

768 Gapais D, Brun JP, Gumiaux C, Cagnard F, Ruffet G, Le Carlier De Veslud C (2015)
769 Extensional tectonics in the Hercynian Armorican belt (France). An overview. *B Soc Geol Fr*
770 186: 117–129

771 García-Arias M, Corretgé LG, Fernández C, Castro A (2015) Water-present melting in the
772 middle crust: The case of the Ollo de Sapo gneiss in the Iberian Massif (Spain). *Chem Geol*
773 419: 176–191

774 Gauthier-Lafaye F, Weber F (2003) Natural nuclear fission reactors: time constraints for
775 occurrence, and their relation to uranium and manganese deposits and to the evolution of the
776 atmosphere. *Precambrian Res* 120: 81–100.

777 Geisler T, Vinx R, Martin-Gombojav N, Pidgeon RT (2005) Ion microprobe (SHRIMP) dating
778 of detrital zircon grains from the quartzites of the Eckergneiss Complex, Harz Mountains
779 (Germany): implications for the provenance and the geological history. *Int J Earth Sci* 94: 369–
780 384

781 Gerdes A, Zeh A (2009) Zircon formation versus zircon alteration — New insights from
782 combined U–Pb and Lu–Hf in-situ LA-ICP-MS analyses, and consequences for the
783 interpretation of Archean zircon from the Central Zone of the Limpopo Belt. *Chem Geol* 261:
784 230–243

785 Gerdes A, Zeh A (2006) Combined U–Pb and Hf isotope LA-(MC-)ICP-MS analyses of detrital
786 zircons: Comparison with SHRIMP and new constraints for the provenance and age of an
787 Armorican metasediment in Central Germany. *Earth Planet Sci Lett* 249: 47–61

788 Georget Y (1986) Nature et origine des granites peralumineux à cordiérite et des roches
789 associées. Exemples des granitoides du Massif Armoricaïn (France): Pétrologie et géochimie.
790 Mémoires Géosciences Rennes 9

791 Gumiaux C, Judenherc S, Brun JP, Gapais D, Granet M, Poupinet G (2004b) Restoration of
792 lithosphere-scale wrenching from integrated structural and tomographic data (Hercynian belt
793 of western France). *Geology* 32: 333–336

794 Gumiaux C, Gapais D, Brun JP, Chantraine J, Ruffet G (2004a) Tectonic history of the
795 Hercynian Armorican Shear belt (Brittany, France). *Geodin Acta* 17: 289–307

796 Höhn S, Koglin N, Klopff L, Schüssler U, Tragelehn H, Frimmel HE, Zeh A, Brätz H (2017)
797 Geochronology, stratigraphy and geochemistry of Cambro-Ordovician, Silurian and Devonian
798 volcanic rocks of the Saxothuringian Zone in NE Bavaria (Germany)—new constraints for
799 Gondwana break up and ocean–island magmatism. *Int J Earth Sci* 1–19

800 Jolivet J, Bienfait G, Vigneresse JL, Cuney M (1989) Heat flow and heat production in Brittany
801 (Western France). *Tectonophysics* 159: 61–72

802 Jones KA, Brown M (1990) High-temperature “clockwise”P-T paths and melting in the
803 development of regional migmatites: an example from southern Brittany, France. *J Metamorph.*
804 *Geol* 8: 551–578

805 Koglin N, Zeh A, Franz G, Schüssler U, Glodny J, Gerdes A, Brätz H (2018) From Cadomian
806 magmatic arc to Rheic ocean closure: The geochronological-geochemical record of nappe
807 protoliths of the Münchberg Massif, NE Bavaria (Germany). *Gondwana Res* 55: 135-152

808 Kretz R (1983) Symbols for rock-forming minerals. *Am Mineral* 68: 277–279

809 Kroner U, Romer RL (2013) Two plates — Many subduction zones: The Variscan orogeny
810 reconsidered. *Gondwana Res* 24: 298–329

811 Laurent O, Couzinié S, Zeh A, Vanderhaeghe O, Moyen JF, Villaros A, Gardien V, Chelle-
812 Michou C (2017) Protracted, coeval crust and mantle melting during Variscan late-orogenic
813 evolution: U–Pb dating in the eastern French Massif Central. *Int J Earth Sci* 1–31

814 Le Fort P, Cuney M, Deniel C, France-Lanord C, Sheppard SMF, Upreti BN, Vidal P (1987)
815 Deep Seated Processes in Collision Zones Crustal generation of the Himalayan leucogranites.
816 *Tectonophysics* 134: 39–57

817 Le Gall B, Authemayou C, Ehrhold A, Paquette JL, Bussien D, Chazot G, Aouizerat A, Pastol
818 Y (2014) LiDAR offshore structural mapping and U/Pb zircon/monazite dating of Variscan
819 strain in the Leon metamorphic domain, NW Brittany. *Tectonophysics* 630: 236–250

820 Le Hébel F (2002) Déformation continentale et histoire des fluides au cours d'un cycle
821 subduction, exhumation, extension. Exemple des porphyroïdes Sud-Armoricains. Dissertation,
822 Université de Rennes 1

823 Linnemann U, Gerdes A, Hofmann M, Marko L (2014) The Cadomian Orogen: Neoproterozoic
824 to Early Cambrian crustal growth and orogenic zoning along the periphery of the West African
825 Craton – Constraints from U-Pb zircon ages and Hf isotopes (Schwarzburg Antiform,
826 Germany). *Precam Res* 244: 236-278

827 Linnemann U, Pereira F, Jeffries TE, Drost K, Gerdes A (2008) The Cadomian Orogeny and
828 the opening of the Rheic Ocean: the diachrony of geotectonic processes constrained by LA-ICP-
829 MS U–Pb zircon dating (Ossa-Morena and Saxo-Thuringian Zones, Iberian and Bohemian
830 Massifs). *Tectonophysics* 461: 21–43

831 López-Moro FJ, López-Plaza M, Gutiérrez-Alonso G, Fernández-Suárez J, López-Carmona A,
832 Hofmann M, Romer RL (2017) Crustal melting and recycling: geochronology and sources of
833 Variscan syn-kinematic anatectic granitoids of the Tormes Dome (Central Iberian Zone). A U–
834 Pb LA-ICP-MS study. *Int J Earth Sci.* <https://doi.org/10.1007/s00531-017-1483-8>

835 Marcoux E (1982) Etude géologique et métallogénique du district plombo-zincifère de Pontivy
836 (Massif armoricain, France): Relations avec les paragenèses stannifères et uranifères. *Bull*
837 *BRGM* (2), section II, n°1: 1-24

838 Marcoux E, Cocherie A, Ruffet G, Darboux JR, Guerrot C (2009) Géochronologie revisitée du
839 dôme du Léon (Massif armoricain, France). *Géologie Fr* 1: 19–40

840 Martínez Catalán JR, Rubio Pascual FJ, Díez Montes A, Díez Fernández RD, Gómez Barreiro
841 J, Dias Da Silva Í, González Clavijo EG, Ayarza P, Alcock JE (2014) The late Variscan HT/LP
842 metamorphic event in NW and Central Iberia: relationships to crustal thickening, extension,
843 orocline development and crustal evolution. *Geol Soc Lond Spec Publ* 405:225–247

844 Matteini M, Pavanetto P, Dabard MP, Hauser N, Loi A, Funedda A (2014) U–Pb ages and Hf
845 isotopes on detrital zircons from Neoproterozoic sediments from the Armorican Massif (NW
846 France): western Gondwana as possible source. 9th South American Symposium on Isotope
847 Geology (SSAGI). 6–9 April 2014, Sao Paulo (Brazil)

848 Michard A, Gurriet P, Soudant M, Albarede F (1985) Nd isotopes in French Phanerozoic shales:
849 external vs. internal aspects of crustal evolution. *Geochim Cosmochim Acta* 49: 601–610

850 Montel JM, Vielzeuf D (1997) Partial melting of metagreywackes, Part II. Compositions of
851 minerals and melts. *Contrib Mineral Petrol* 128: 176–196

852 Montel JM (1993) Geochemistry of Accessory Minerals A model for monazite/melt
853 equilibrium and application to the generation of granitic magmas. *Chem Geol* 110: 127–146.

854 Nance DR, Murphy BJ (1994) Contrasting basement isotopic signatures and the palinspastic
855 restoration of peripheral orogens: An example from the Neoproterozoic Avalonian-Cadomian
856 belt. *Geology* 22: 617-620

857 Patiño-Douce AE (1999) What do experiments tell us about the relative contributions of crust
858 and mantle to the origin of granitic magmas? *Geol Soc Lond Spec Publ* 168: 55–75.

859 Patiño-Douce AE and Johnston AD (1991) Phase equilibria and melt productivity in the pelitic
860 system: implications for the origin of peraluminous granitoids and aluminous granulites.
861 *Contrib. Mineral Petrol* 107: 202–218

862 Peiffert C, Nguyen-Trung C, Cuney M (1996) Uranium in granitic magmas: Part 2.
863 Experimental determination of uranium solubility and fluid-melt partition coefficients in the
864 uranium oxide-haplogranite-H₂O-NaX (X = Cl, F) system at 770°C, 2 kbar. *Geochim*
865 *Cosmochim Acta* 60: 1515–1529

866 Peiffert C, Cuney M, Nguyen-Trung C (1994) Uranium in granitic magmas: Part 1.
867 Experimental determination of uranium solubility and fluid-melt partition coefficients in the
868 uranium oxide-haplogranite-H₂O-Na₂CO₃ system at 720–770°C, 2 kbar. *Geochim Cosmochim*
869 *Acta* 58: 2495–2507.

870 Pelhate A (1994) Carboniferous of the Armorican Massif. In: Chantraine J, Rolet J, Santallier
871 DS, Piqué A, Keppie JD (eds) *Pre-Mesozoic Geology in France and Related Areas*. Springer,
872 Berlin, Heidelberg, pp 162-168

873 Pochon A, Poujol M, Gloaguen E, Branquet Y, Cagnard F, Gumiaux C, Gapais D (2016). U-
874 Pb LA-ICP-MS dating of apatite in mafic rocks: Evidence for a major magmatic event at the
875 Devonian-Carboniferous boundary in the Armorican Massif (France). *Am Mineral* 101: 2430-
876 2442

877 Peucat JJ, Auvray B, Hirbec Y, Calvez JY (1984) Granites et cisaillements hercyniens dans le
878 Nord du Massif Armoricaïn; géochronologie Rb-Sr. *Bull. B Soc Geol Fr* S7–XXVI: 1365–1373

879 Raith JG (1995) Petrogenesis of the Concordia Granite Gneiss and its relation to W-Mo
880 mineralization in western Namaqualand, South Africa. *Precambrian Res* 70: 303–335

881 Robb LJ (1986) Uraniferous leucogranites from the Namaqualand Metamorphic Complex: Part
882 I—Geology, geochemistry and petrogenesis. *Mineral Deposits of Southern Africa* 2: 1609-1627

883 Robb LJ, Armstrong RA, Waters DJ (1999) The History of Granulite-Facies Metamorphism
884 and Crustal Growth from Single Zircon U–Pb Geochronology: Namaqualand, South Africa. *J*
885 *Petrol* 40: 1747–1770

886 Romer RL, Kroner U (2016) Phanerozoic tin and tungsten mineralization—Tectonic controls
887 on the distribution of enriched protoliths and heat sources for crustal melting. *Gondwana Res*
888 31: 60–95

889 Romer RL, Kroner U (2015). Sediment and weathering control on the distribution of Paleozoic
890 magmatic tin–tungsten mineralization. *Miner Deposita* 50: 327–338

891 Romer RL, Schneider J, Linnemann U (2010) Post-Variscan deformation and hydrothermal
892 mineralization in Saxo-Thuringia and beyond: a geochronologic review in Linnemann U,
893 Romer RL (eds) *Pre-Mesozoic Geology of Saxo-Thuringia – From the Cadomian Active*
894 *Margin to the Variscan Orogen*, Schweizerbart, Stuttgart, pp 347-360

895 Romer RL, Thomas R, Stein HJ, Rhede D (2007) Dating multiply overprinted Sn-mineralized
896 granites—examples from the Erzgebirge, Germany. *Miner Deposita* 42: 337–359

897 Rudnick RL, Gao S (2003) Composition of the continental crust. *Treatise on geochemistry* 3

898 Samson SD, D’lemos RS (1998) U–Pb geochronology and Sm–Nd isotopic composition of
899 Proterozoic gneisses, Channel Islands, UK. *J Geol Soc* 155: 609–618

900 Scherer E, Münker C, Mezger K (2001) Calibration of the Lutetium-Hafnium Clock. *Science*
901 293: 683–687

902 Söderlund U, Patchett PJ, Vervoort JD, Isachsen CE (2004) The ^{176}Lu decay constant
903 determined by Lu–Hf and U–Pb isotope systematics of Precambrian mafic intrusions. *Earth*
904 *Planet Sci Lett* 219: 311–324

905 Shaw RA, Goodenough KM, Roberts NM, Horstwood MS, Chenery SR, Gunn AG (2016)
906 Petrogenesis of rare-metal pegmatites in high-grade metamorphic terranes: A case study from
907 the Lewisian Gneiss Complex of north-west Scotland. *Precambrian Res* 281: 338-62

908 Tartèse R, Boulvais P (2010) Differentiation of peraluminous leucogranites “en route” to the
909 surface. *Lithos* 114: 353–368

910 Tartèse R, Boulvais P, Poujol M, Gloaguen E, Cuney M (2013) Uranium Mobilization from the
911 Variscan Questembert Syntectonic Granite During Fluid-Rock Interaction at Depth. *Econ Geol*
912 108: 379–386.

913 Tartèse R, Boulvais P, Poujol M, Chevalier T, Paquette JL, Ireland TR, Deloule E (2012)
914 Mylonites of the South Armorican Shear Zone: Insights for crustal-scale fluid flow and water–
915 rock interaction processes. *J Geodyn* 56–57: 86–107

916 Tartèse R, Ruffet G, Poujol M, Boulvais P, Ireland TR (2011b) Simultaneous resetting of the
917 muscovite K-Ar and monazite U-Pb geochronometers: a story of fluids. *Terra Nova* 23: 390–
918 398

919 Tartèse R, Poujol M, Ruffet G, Boulvais P, Yamato P, Košler J (2011a) New U-Pb zircon and
920 $^{40}\text{Ar}/^{39}\text{Ar}$ muscovite age constraints on the emplacement of the Lizio syn-tectonic granite
921 (Armorican Massif, France). *Comptes Rendus Geosci* 343: 443–453

922 Taylor SR, McLennan SM (1985) *The continental crust: Its composition and evolution*

923 Thiéblemont D, Cataing C, Billa M, Bouton P, Prémat (2009) Notice explicative de la Carte
924 géologique et des Ressources minérales de la République Gabonaise à 1: 1 000 000. Editions
925 DGMG - Ministère des Mines, du Pétrole, des Hydrocarbures, Libreville

926 Thomas RJ, De Beer CH, Bowring SA (1996) A comparative study of the Mesoproterozoic late
927 orogenic porphyritic granitoids of southwest Namaqualand and Natal, South Africa. *J Afr Earth*
928 *Sci* 23: 485–508

929 Tichomirowa M, Sergeev S, Berger HJ, Leonhardt D (2012) Inferring protoliths of high-grade
930 metamorphic gneisses of the Erzgebirge using zirconology, geochemistry and comparison with
931 lower-grade rocks from Lusatia (Saxothuringia, Germany). *Contrib Mineral Petrol* 164: 375-
932 396

933 Tischendorf G, Förster HJ (1994) Hercynian granite magmatism and related metallogenesis in
934 the Erzgebirge: A status report. *Mineral deposits of the Erzgebirge/Krusne hory*
935 (Germany/Czech Republic). *Monogr Ser Mineral Deposits* 31: 5-23

936 Trautmann F, Carn, A (1997) La Guerche-De-Bretagne 354, Carte géologique de France 1:50
937 000. BRGM

938 Turpin L, Cuney M, Friedrich M, Bouchez JL, Aubertin M (1990) Meta-igneous origin of
939 Hercynian peraluminous granites in N.W. French Massif Central: implications for crustal
940 history reconstructions. *Contrib Mineral Petrol* 104: 163–172

941 Vermeesch P (2012) On the visualisation of detrital age distributions. *Chem Geol* 312: 190–
942 194

943 Vernhet Y, Plaine J, Trautmann F, Pivette B (2009) Cossé-Le-Vivien 355, Carte géologique de
944 France 1:50 000. BRGM

945 Vidal M, Dabard MP, Gourvenec R, Le Hérisse A, Loi A, Paris F, Plusquellec Y, Racheboeuf
946 PR (2011) Le Paléozoïque de la presqu'île de Crozon, Massif armoricain (France). *Géologie de*
947 *la France* 1: 3-45

948 Vidal P, Auvray B, Charlot R, Cogné J (1981). Precadomian relicts in the Armorican Massif:
949 Their age and role in the evolution of the western and central European Cadomian-Hercynian
950 belt. *Precambrian Res* 14: 1-20

951 Vielzeuf D, Holloway JR (1988) Experimental determination of the fluid-absent melting
952 relations in the pelitic system. *Contrib Mineral Petrol* 98: 257–276

953 Vigneresse JL, Cuney M, Jolivet J, Bienfait G (1989) Selective heat-producing element
954 enrichment in a crustal segment of the mid-European Variscan chain. *Tectonophysics* 159: 47–
955 60

956 Villaseca C, Martínez EM, Orejana D, Andersen T, Belousova E (2016) Zircon Hf signatures
957 from granitic orthogneisses of the Spanish central system: Significance and sources of the
958 Cambro-Ordovician magmatism in the Iberian Variscan Belt. *Gondwana Res* 34: 60-83

959 Villaseca C, Orejana D, Belousova EA (2012) Recycled metagneous crustal sources for S- and
960 I-type Variscan granitoids from the Spanish Central System batholith: Constraints from Hf
961 isotope zircon composition. *Lithos* 153: 84–93

962 Watson EB, Harrison TM (1983) Zircon saturation revisited: temperature and composition
963 effects in a variety of crustal magma types. *Earth Planet Sci Lett* 64: 295–304

964 Wedepohl KH (2016) Chemical composition and fractionation of the continental crust. *Geol*
965 *Rundsch* 80: 207–223

966 Zeh A, Gerdes A (2010) Baltica- and Gondwana-derived sediments in the Mid-German
967 Crystalline Rise (Central Europe): Implications for the closure of the Rheic ocean.
968 *Gondwana Res* 17: 254–263

969 Zeh A, Brätz H, Millar I L, Williams IS (2001) A combined zircon SHRIMP and Sm-

970 Nd isotope study on high-grade paragneisses from the Mid-German Crystalline Rise:
971 Evidence for northern Gondwanan and Grenvillian provenance. *J Geol Soc London*,
972 158: 983-994

973 Captions

974 Fig.1: Schematic representation of the west European Variscan belt representing the main terranes
975 (Ballèvre et al. 2009, 2014; Ballèvre 2016) and showing the distribution of U deposits (Cuney and Kyser
976 2008), Variscan granitoids and Early Paleozoic felsic to intermediate igneous rocks (after the 1:1 000
977 000 geological maps of France [Chantraine et al. 2003], Portugal and Spain [Civis Llovera (2015)] and
978 the 1:500 000 geological maps of Czechoslovakia [Fusán et al. 1967] and Czech Republic [Cháb et al.
979 2007]). The granitoids typology is from Barbarin (1999). MPG: muscovite-bearing peraluminous
980 granites; CPG: cordierite-bearing peraluminous granitoids; KCG: K-rich and K-feldspar porphyritic
981 calc-alkaline granitoids. ACG: amphibole-rich calc-alkaline granitoids. NASZ: North Armorican shear
982 zone; NBSASZ: northern branch of the south Armorican shear zone; SBSASZ: southern branch of the
983 south Armorican shear zone. NEF: Nort-sur-Erdre fault. Mineral abbreviations according to Kretz
984 (1983).

985

986 Fig. 2: (a) principal structural domains from the Armorican Massif. (b) General geological map of the
987 Armorican Massif [modified from Chantraine et al. (2003), Gapais et al. (2015) and Ballouard et al.
988 (2017b, in press)] identifying the different types of Carboniferous granitoids after Barbarin (1999) and
989 Capdevila (2010) and localizing the U deposits (<http://infoterre.brgm.fr>). The high heat production and
990 flow belt (HHPFB) from Vignerresse et al. (1989) and Jolivet et al. (1989) is indicated. Locality numbers
991 are referenced in Table 1. NASZ: north Armorican shear zone; NBSASZ: northern branch of the South
992 Armorican shear zone; SBSASZ: southern branch of the south Armorican shear zone. Fe-K granites:
993 ferro-potassic granites. Mg-K granites: magnesio-potassic granites. Mineral abbreviations according to
994 Kretz (1983).

995

996 Fig. 3: A/NK [$Al_2O_3 / (Na_2O + K_2O)$] versus A/CNK [$Al_2O_3 / (CaO + Na_2O + K_2O)$] diagram (molar
997 proportion) reporting the composition of Late Carboniferous MPGs from the Armorican Massif. Data

998 are from Ballouard et al. (2015a, 2017a), Euzen (1993), Georget (1986), Tartèse and Boulvais (2010),
999 Tartèse et al. (2012) and this study.

1000

1001 Fig. 4: U versus Th diagram reporting the whole-rock composition of Late Carboniferous MPGs from
1002 the Armorican Massif and their potential sources. Data are from this study, Georget (1986), Vignerresse
1003 et al. (1989), Euzen (1993), Béchenec et al. (1996, 1999, 2001), Trautmann and Carn (1997), Dabard
1004 and Peucat (2001), Le Hébel (2002), Tartèse and Boulvais (2010), Béchenec and Thiéblement (2013),
1005 Tartèse et al. (2012) and Ballouard et al. (2015a, 2017b). The average U content (2.7 ppm) and Th/U
1006 value (~4) of the upper continental crust (UCC; Rudnick and Gao 2003) are indicated.

1007

1008 Fig. 5: Initial Sr and Nd isotopic composition calculated at 315 Ma of Late Carboniferous MPGs from
1009 the Armorican Massif (Data from this study; Ballouard et al. 2015a, 2017b; Tartèse and Boulvais 2010).
1010 The yellow double arrow represents the $\epsilon_{\text{Nd}}(315 \text{ Ma})$ composition of the Langonnet MPG (Ballouard
1011 et al. 2017b) whereas other vertical bars represent the $\epsilon_{\text{Nd}}(315 \text{ Ma})$ composition of Cambro-Ordovician
1012 peraluminous igneous rocks [acid (meta)volcanics: Ballèvre et al. 2012; (meta)granitoids: Ballouard et
1013 al. 2017b] as well as Brioverian (Dabard et al. 1996; Dabard 1997) and Paleozoic (Michard et al. 1985;
1014 Dabard and Peucat 2001; this study) sediments. The composition of ca. 2000 Ma Icartian orthogneisses
1015 from the Channel Islands (black arrow) is out of the diagram with $\epsilon_{\text{Nd}}(315 \text{ Ma})$ values between -18 and
1016 -14 (Samson and D'Lemos 1998). The grey dashed arrow represents the north-south evolution of the
1017 MPG isotopic composition. Sm-Nd isotopic composition of CHUR from Bouvier et al. (2008).

1018

1019 Fig. 6: Representative cathodoluminescence pictures of zircon grains from MPGs, sediments and
1020 Cambro-Ordovician metagranitoids of the Armorican Massif analyzed during this study. Dashed circles
1021 represent the location of LA-ICP-MS U-Pb analyses. The corresponding U-Pb dates (1σ uncertainty)
1022 and $\epsilon_{\text{Hf}}(t)$ values are indicated. All zircon grains are shown at the same scale and the scale bar is
1023 indicated in the upper right corner. Carbon. = Carboniferous.

1024

1025 Figure 7: Histogram and Kernel density estimates (KDE) of U-Pb dates obtained on inherited zircon
1026 grains from Late Carboniferous MPGs of the Armorican Massif. Number in grey inside the diagrams
1027 corresponds to the age of peaks (Ma) obtained by KDE. Zones in color represent the main period of
1028 inheritance.

1029

1030 Fig. 8: Histogram and Kernel density estimates (KDE) of U-Pb dates obtained on detrital zircon grains
1031 from sedimentary rocks of the Armorican Massif. Zones in color represent the main period of inheritance
1032 recorded by zircon from the Late Carboniferous MPGs.

1033

1034 Fig. 9: Histogram and Kernel density estimates (KDE) of U-Pb dates obtained on zircon grains from
1035 Cambro-Ordovician and Early Carboniferous peraluminous igneous rocks of the Armorican Massif.
1036 Zones in color represent the main period of inheritance recorded by zircon from the Late Carboniferous
1037 MPGs.

1038

1039 Fig. 10: $\epsilon\text{Hf}(t)$ versus U-Pb ages for (a) inherited zircon grains from Late Carboniferous MPGs, (b)
1040 detrital zircon from sediments (c) magmatic zircon from Early Paleozoic metagranitoids and (d) zircon
1041 from Late Carboniferous MPGs and their potential sources. In (d), the composition of magmatic zircon
1042 from Early Variscan granitoids is extrapolated using Devonian-Carboniferous zircon from Lower
1043 Carboniferous sediments. The main origin of zircon grains is indicated: WA = West African craton, G
1044 = Grenvillian belt, CA = Cadomian-Avalonian belt, R = Cambro-Ordovician Rift, EV = Early Variscan.
1045 The crustal evolution trends are calculated using a $^{176}\text{Lu}/^{177}\text{Hf}$ ratio of 0.0113 (Taylor and McLennan
1046 1985; Wedepohl 2016). Data for the Pontivy and Langonnet MPG are from Ballouard et al. (2017b)
1047 whereas other data are from this study.

1048

1049 Fig.11: U versus Th diagram reporting the whole-rock composition of granitoids from (a) the Archean
1050 Gabonese craton and (b) Mesoproterozoic western Namaqualand province, South Africa.
1051 Geochronological and Geochemical data for Gabon are from Bouton et al. (2009) and Thiéblemont et
1052 al. (2009) whereas data for Namaqualand are from Robb (1986, 1999), Raith (1995), Thomas et al.
1053 (1996), Clifford et al. (2004), Andreoli et al. (2006), Bailie et al. (2007) and Duchesne et al. (2007). The
1054 average U content (2.7 ppm) and Th/U value (~4) of the upper continental crust (UCC; Rudnick and
1055 Gao 2003) are indicated.

1056

1057 Table 1: summary of zircon U-Pb data. Pop. = population.

Figure 1

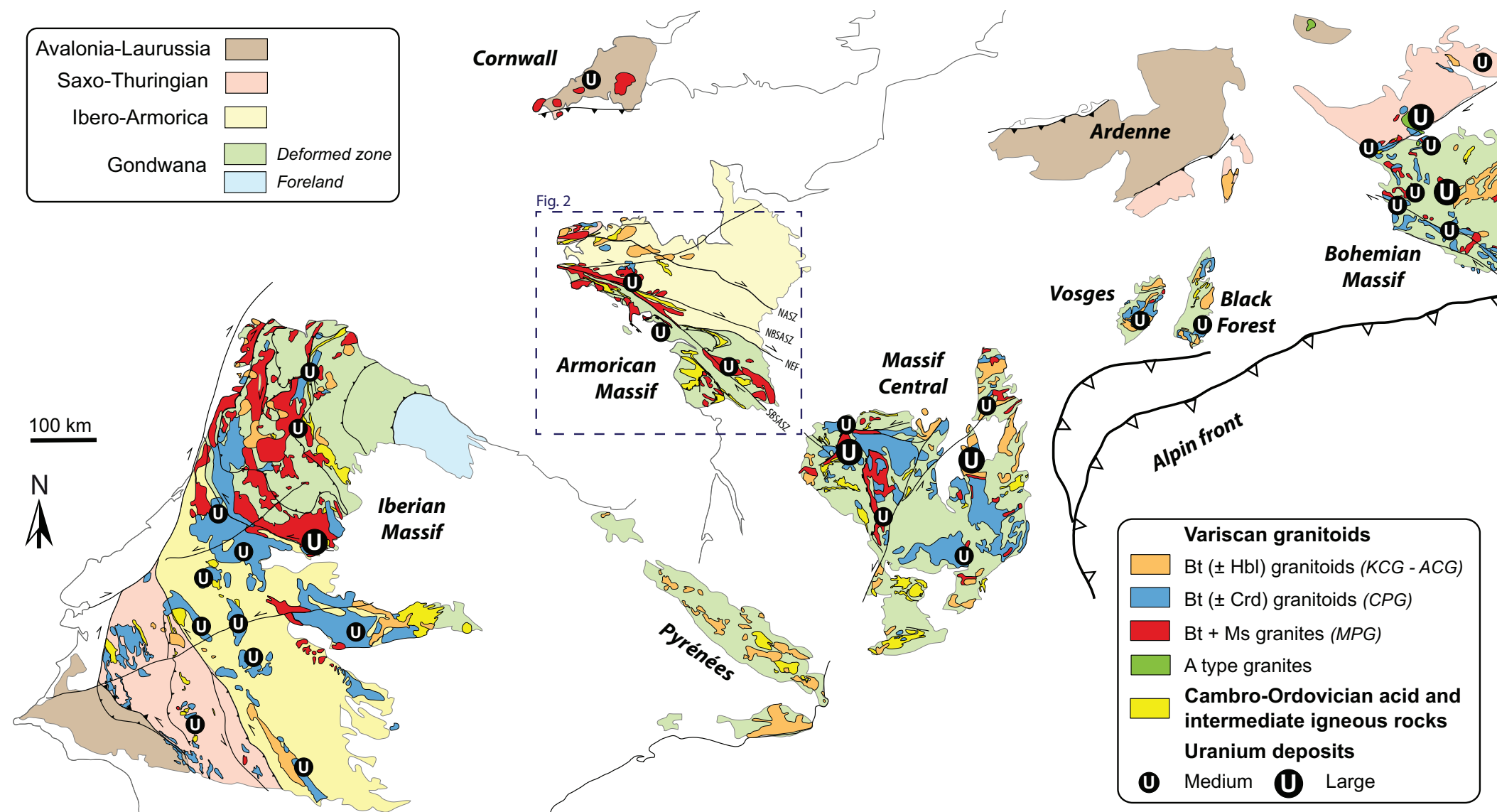


Figure 2

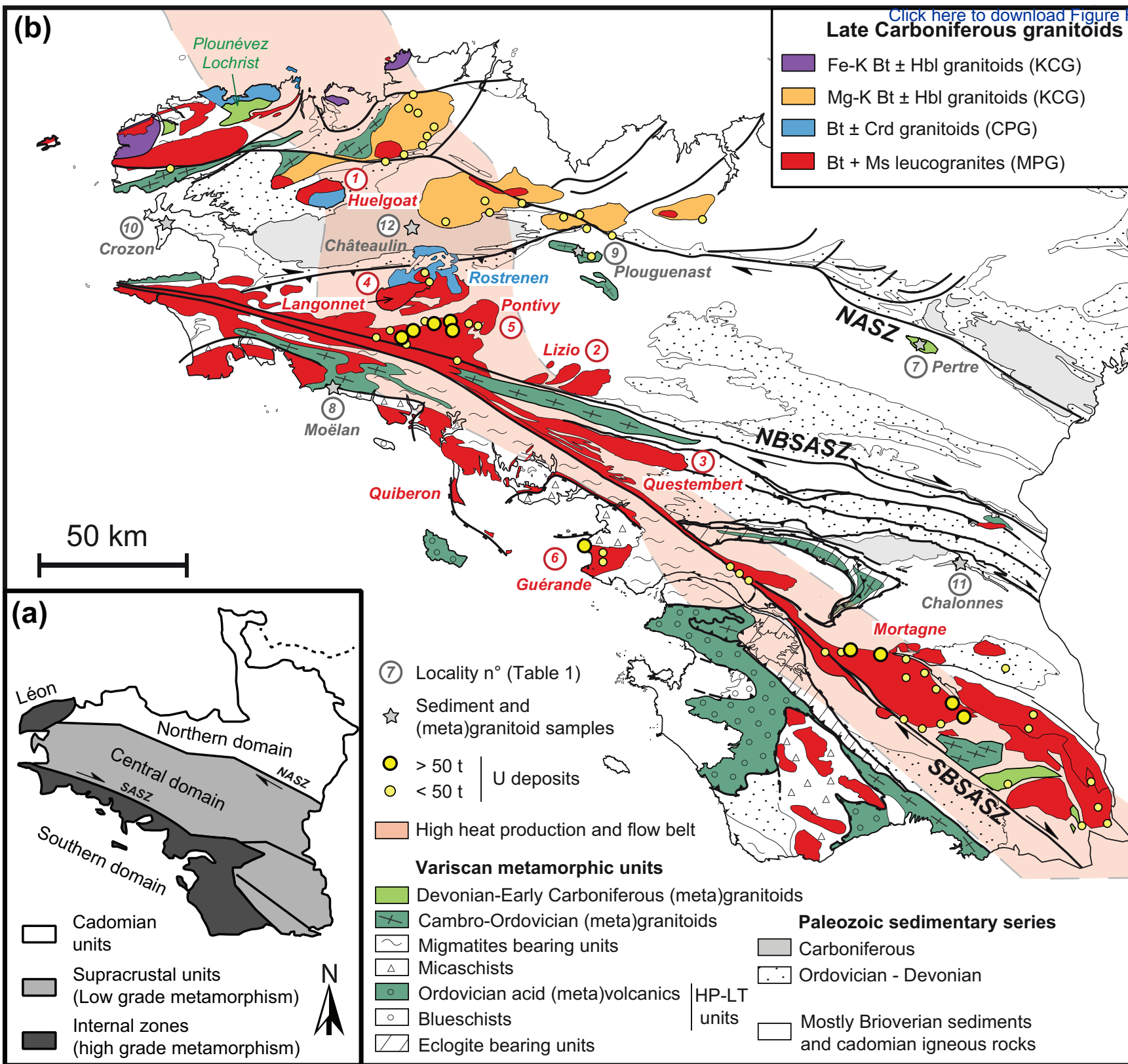
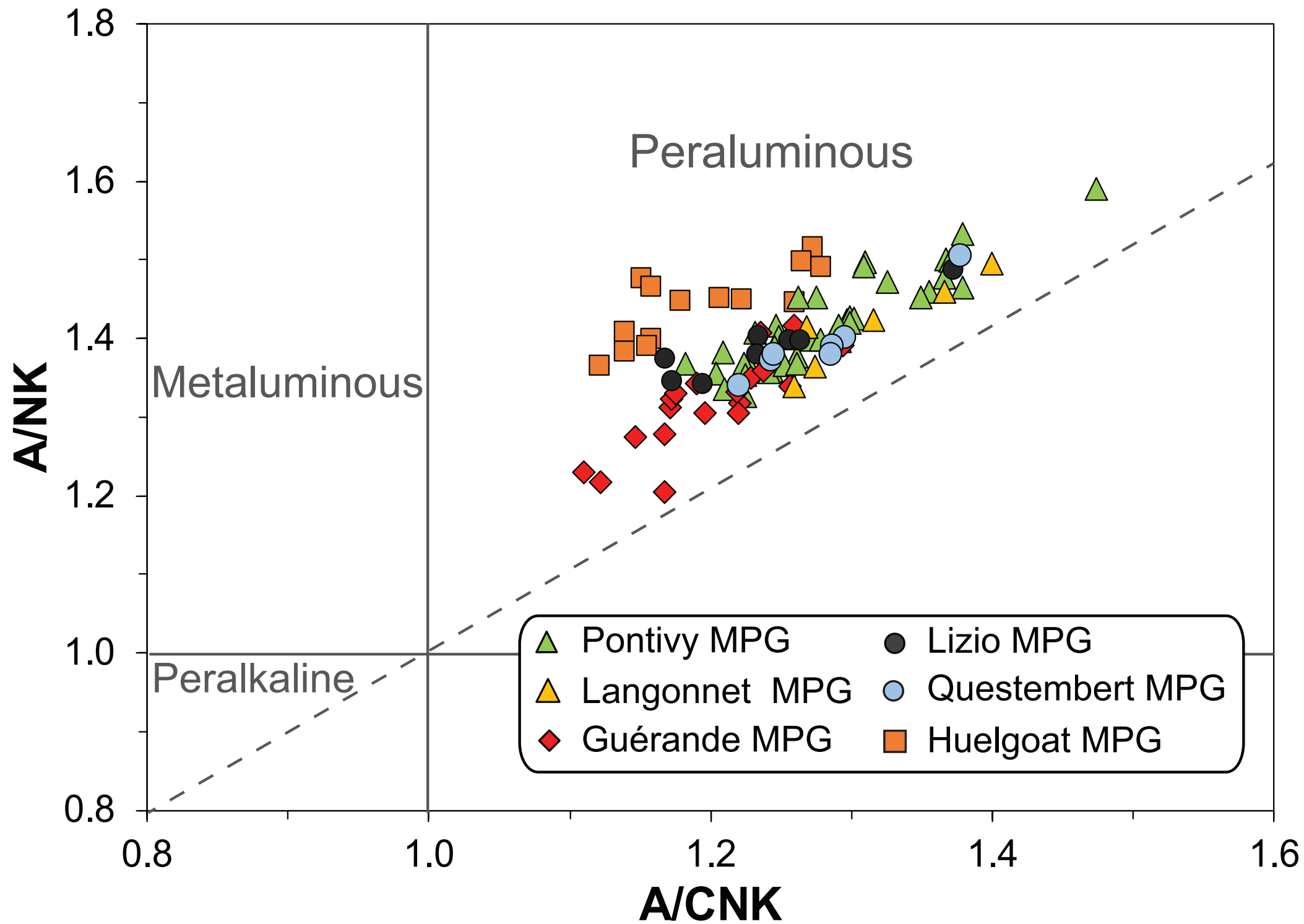
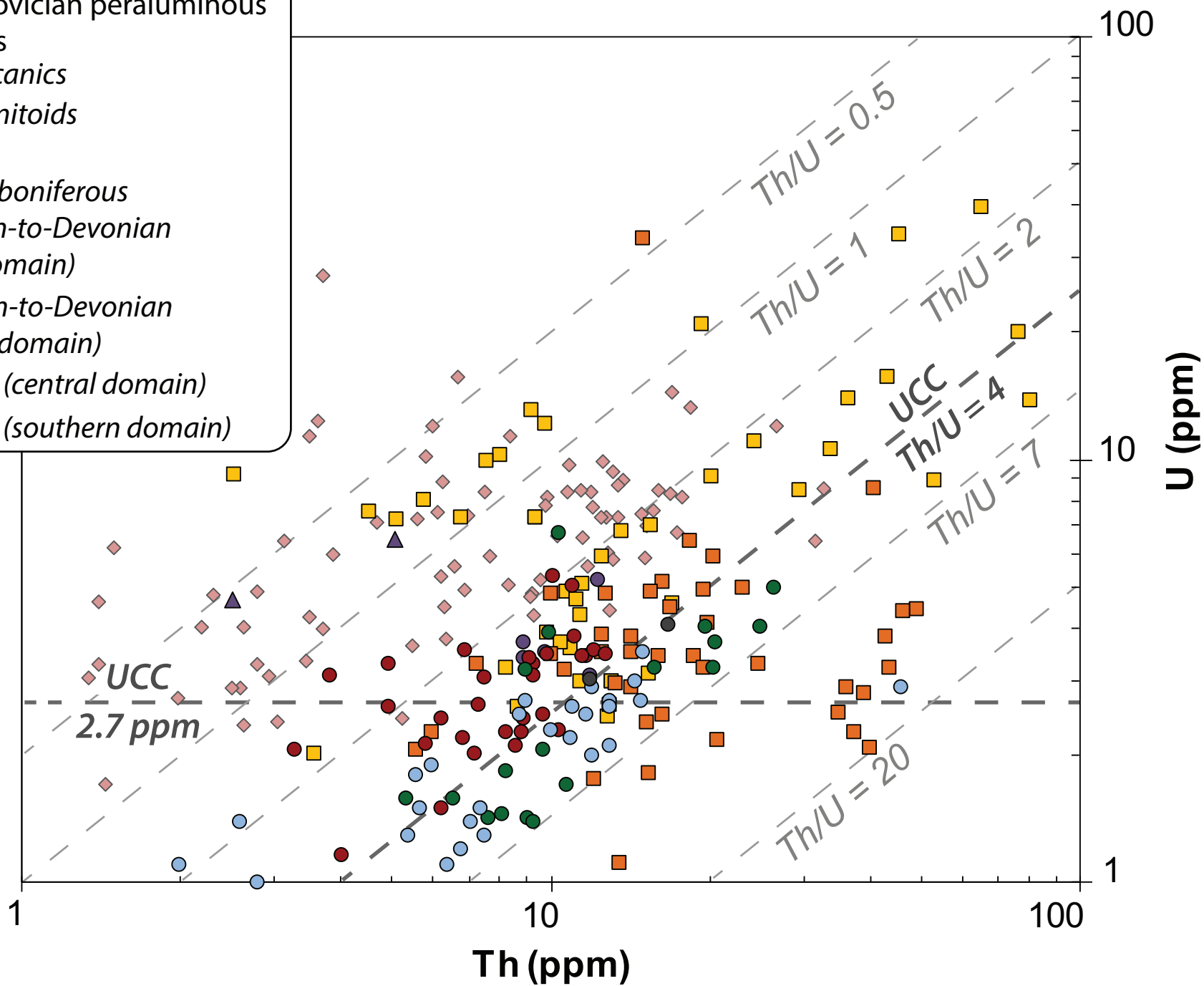


Figure 3



- Late Carboniferous igneous rocks
 ◆ *MPGs*
- Early Carboniferous igneous rocks
 ▲ *Pertre MPG*
- Cambro-Ordovician peraluminous igneous rocks
 ■ *(Meta)volcanics*
 ■ *(Meta)granitoids*
- Sediments
 ● *Lower Carboniferous*
 ● *Ordovician-to-Devonian (central domain)*
 ● *Ordovician-to-Devonian (southern domain)*
 ● *Brioverian (central domain)*
 ● *Brioverian (southern domain)*



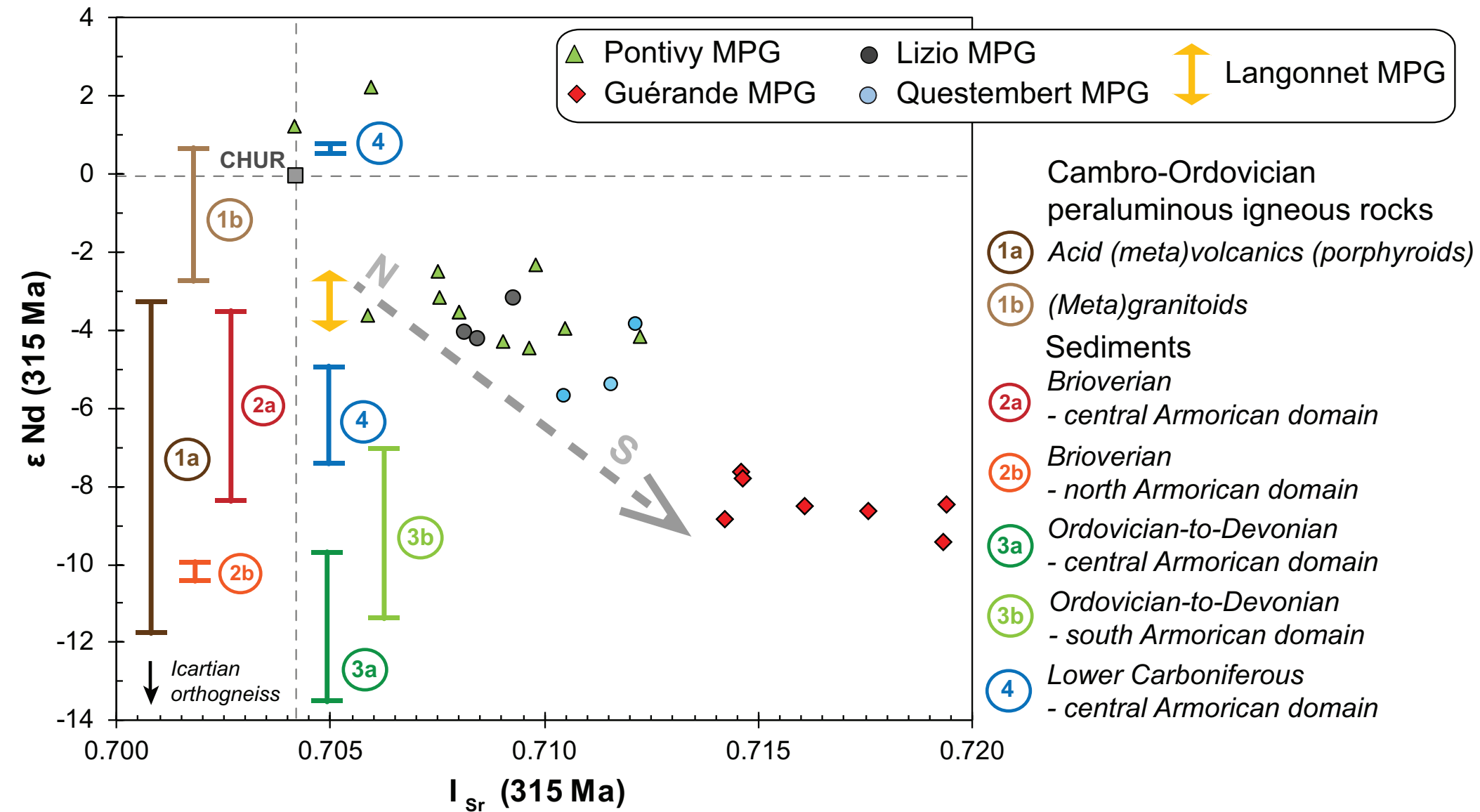




Figure 7

[Click here to download Figure Figure 7.eps](#)

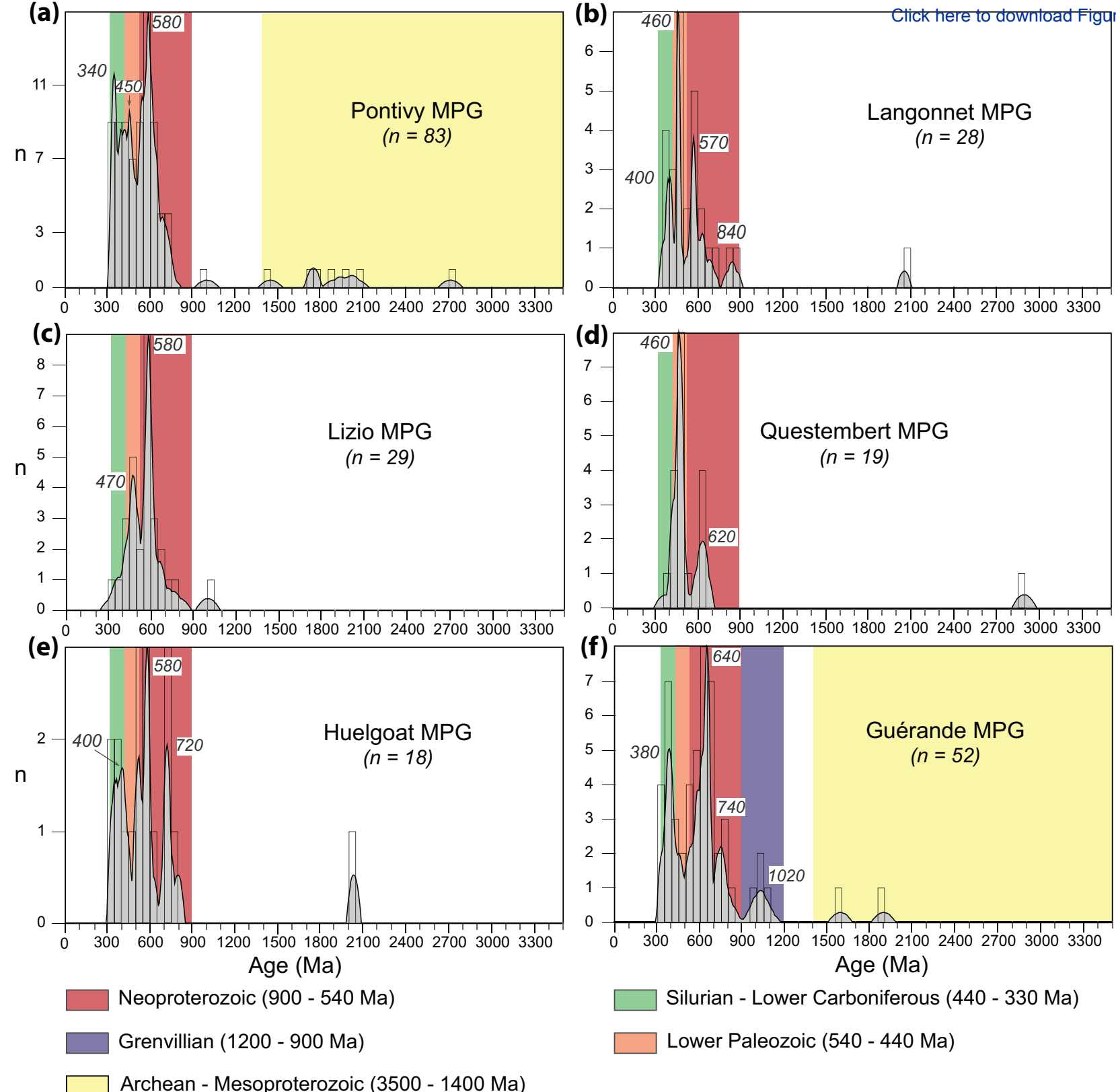


Figure 8

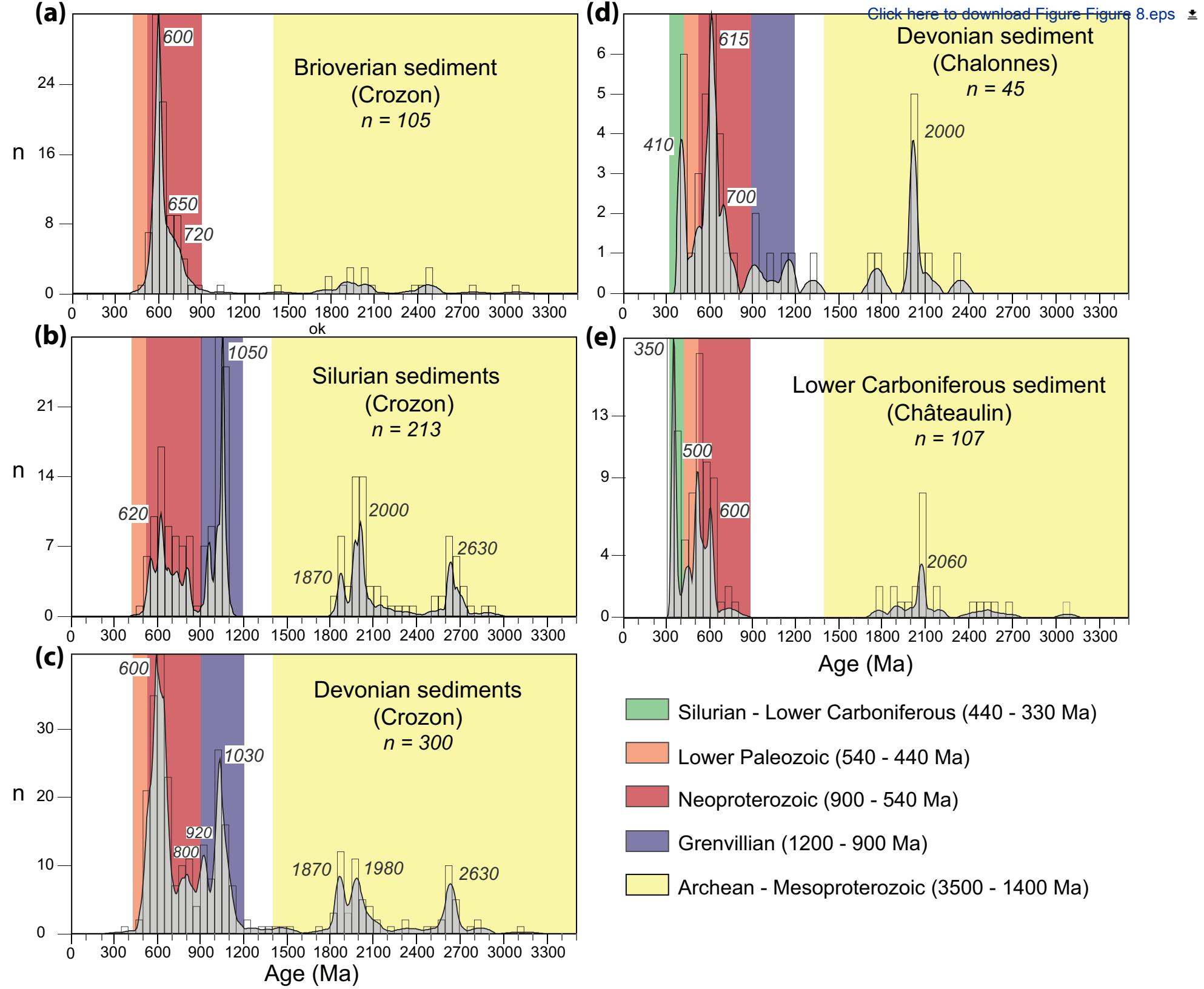
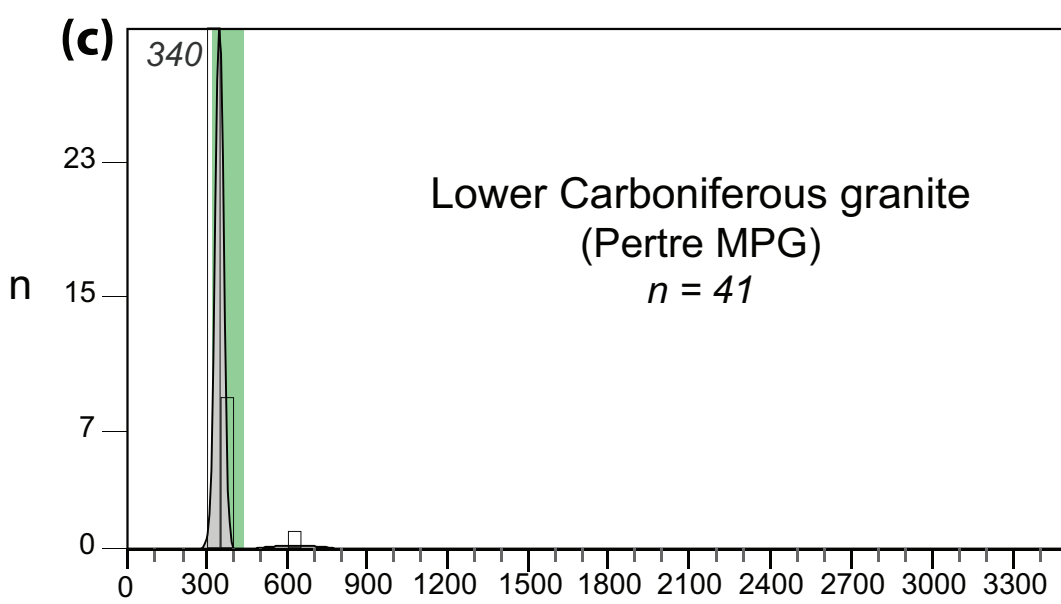
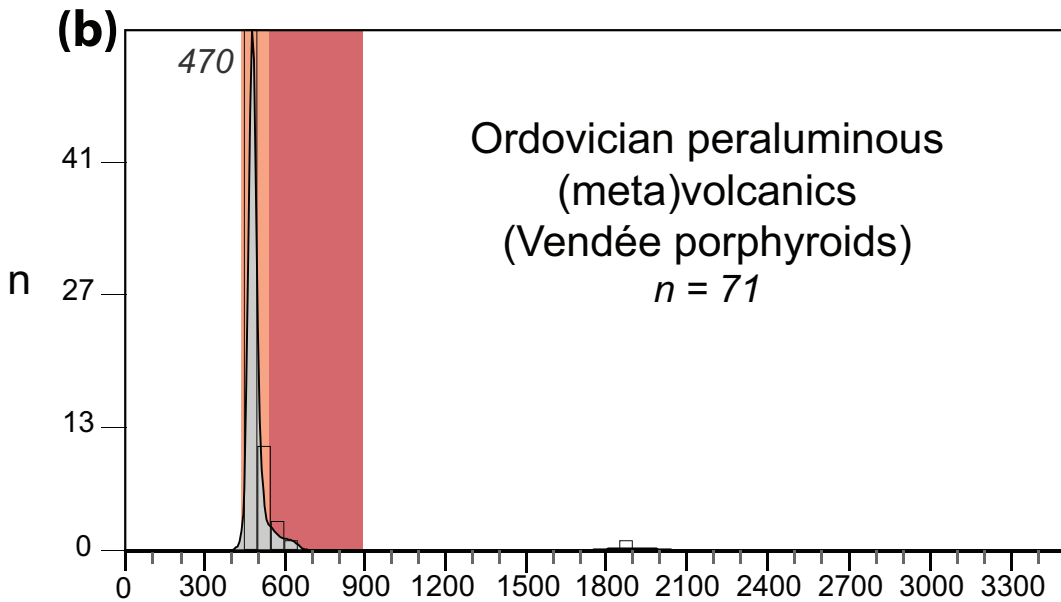
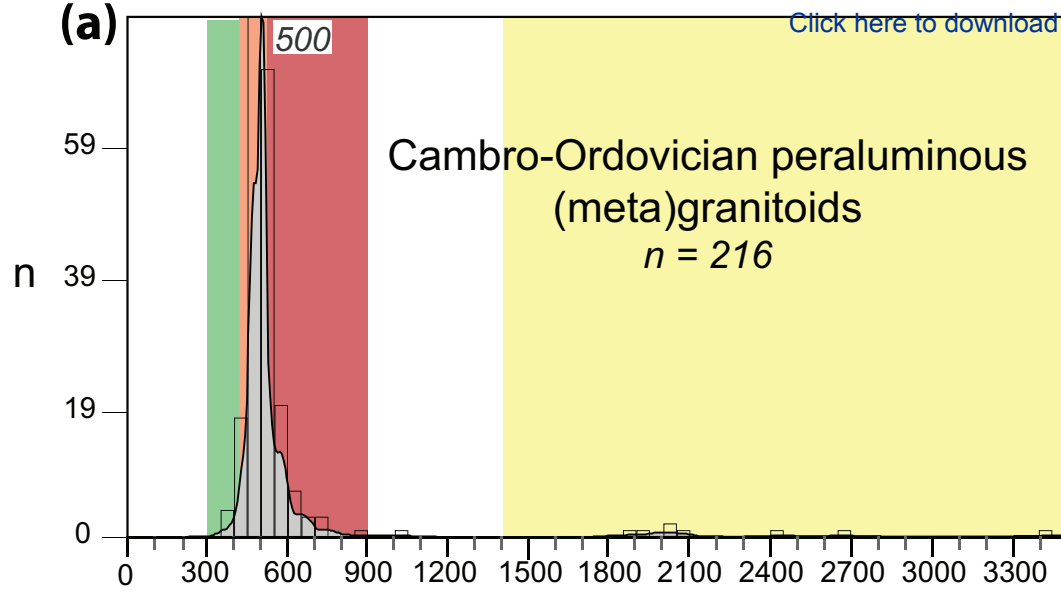



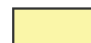
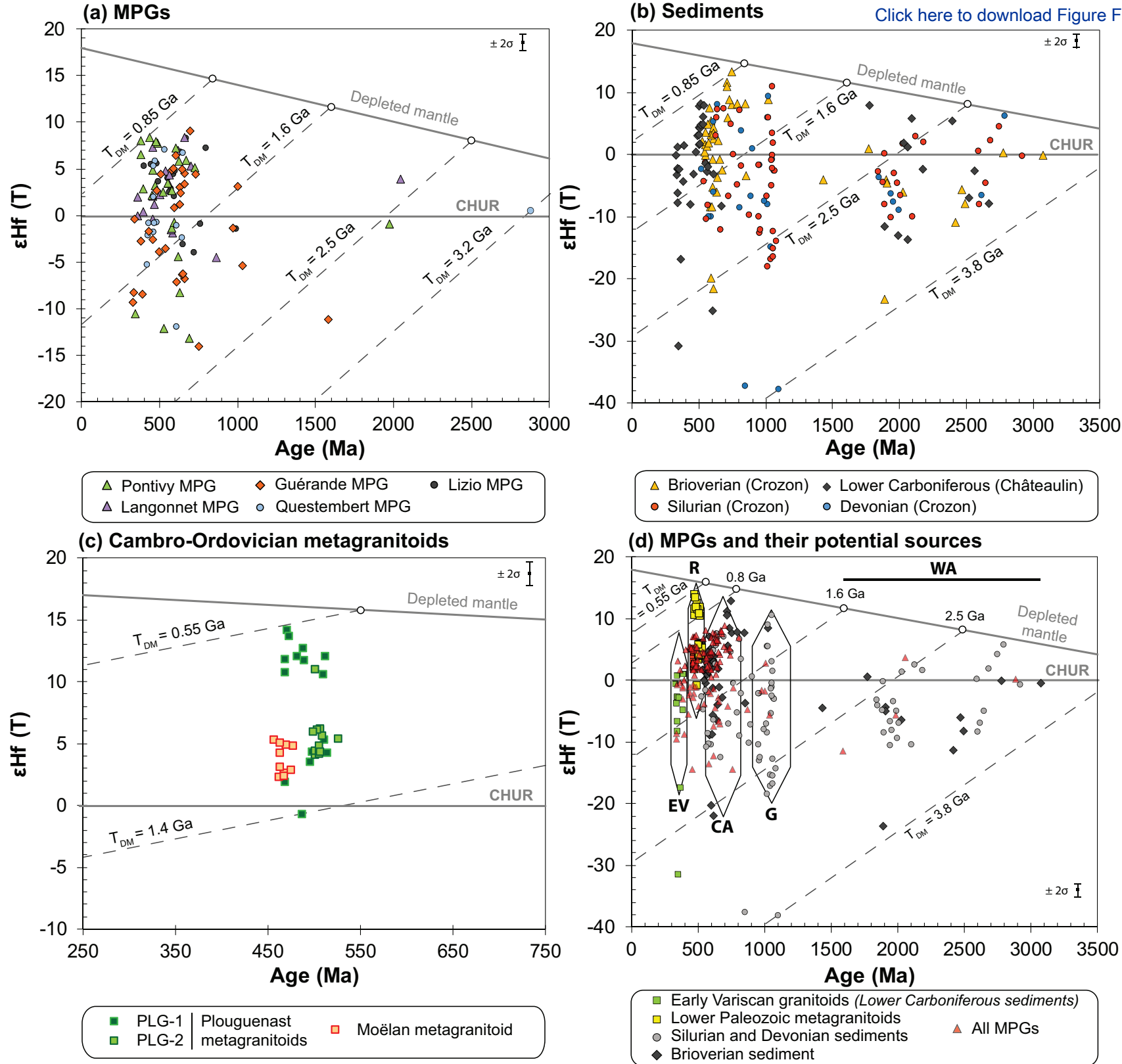


Figure 9



-  Silurian - Lower Carboniferous (440 - 330 Ma)
-  Lower Paleozoic (540 - 440 Ma)
-  Neoproterozoic (900 - 540 Ma)
-  Archean - Mesoproterozoic (3500 - 1400 Ma)



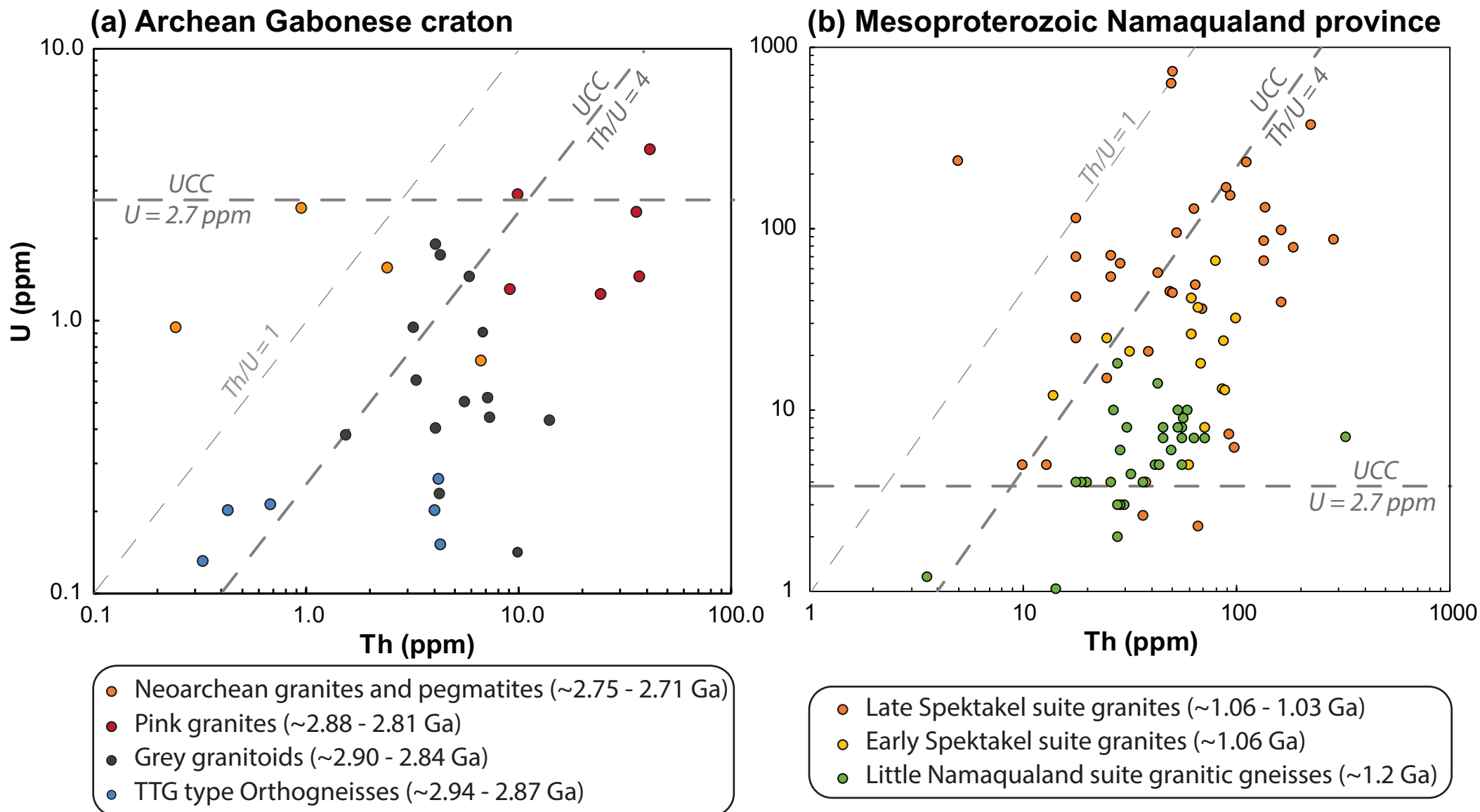


Table 1

Reference	Sample	Locality / intrusion name	Reference N° in Figure 2	Rock type	Intrusion / deposition age	Number U-Pb / Hf	Pop. 1 (%)	Pop. 2 (%)	Pop. 3 (%)	Pop. 4 (%)	Pop. 5 (%)
							3500 – 1400 Ma	1200 – 900 Ma	900 – 540 Ma	540 – 440 Ma	440 – 330 Ma
This study	LOC-1	Châteaulin basin	12	Sandstone	Lower Carboniferous	107 / 45	22	0	23	22	32
This study	CRO-2	Crozon	10	Sandstone	Upper Devonian	300 / 27	23	24	46	6	0
	CRO-1			Sandstone-siltstone	Middle Devonian						
	CRO-12 CRO-11			Sandstone	Lower Devonian						
Ducassou et al. (2014)	DevSA2	Chalonnnes	11	Sandstone	Devonian	45 / 0	24	11	42	7	13
This study	CRO-6	Crozon	10	Sandstone	Silurian	213 / 54	36	32	29	3	0
	CRO-3			Sandstone-siltstone							
This study	CRO-9	Crozon	10	Sandstone	Brioverian	105 / 48	17	1	78	4	0
This study	PLG-1	Plouguenast	9	Metagranitoid (MPG)	Ordovician (477.9 ± 2.9 Ma)	216 / 37	4	0	18	71	7
	PLG-2			Metagranitoid (tonalite)	Cambrian (504.5 ± 1.8 Ma)						
	PLG-3			MPG	Ordovician						
	PLG-4 QIMP-1	Moëlan	8	Metagranitoid (tonalite) Metagranitoid (tonalite)	Ordovician (486.7 ± 8.8 Ma) Ordovician (466.2 ± 3.6 Ma)						
Ballèvre et al. (2012)	FL-31	Bréthomé		Felsic (meta)volcanics	Ordovician (472 ± 4 Ma)	71 / 0	1	0	6	93	0
	CG13a	Chie-Loup			Ordovician (486 ± 4 Ma)						
	CG5	Mareuil / Lay			Ordovician (478 ± 2 Ma)						
	CG09	La Sauzaie			Ordovician (491 ± 12 Ma)						
	FI2a	Sauzon			Ordovician (494 ± 4 Ma)						
Vernhet et al. (2012)	Pertre 1	Pertre	7	MPG	Lower Carboniferous (345 ± 3 Ma)	41 / 0	0	0	2	0	93
	Pertre 4				Lower Carboniferous (348 ± 19 Ma)						
	Pertre 6				Lower Carboniferous (340 ± 2 Ma)						
Ballouard et al. (2015)	GUE-3	Guérande	6	MPG	Upper Carboniferous (309.4 ± 1.9 Ma)	52 / 32	4	8	50	13	25
This study	GUE-4				Upper Carboniferous (309.7 ± 1.3 Ma)						
GUE-5	Upper Carboniferous (302.5 ± 1.6 Ma)										
Ballouard et al. (2017b)	PONT-1	Pontivy	5	MPG	Upper Carboniferous (316.7 ± 2.5 Ma)	83 / 24	8	1	39	20	31
This study	PONT-10				Upper Carboniferous						
	PONT-14				Upper Carboniferous						
	PONT-15				Upper Carboniferous						
	PONT-26				Upper Carboniferous (310.3 ± 4.7 Ma)						
Ballouard et al. (2017b)	PONT-20	Langonnet	4	MPG	Upper Carboniferous (304.7 ± 2.7 Ma)	28 / 18	4	0	39	32	25
This study	QRT-08	Questembert	3	MPG	Upper Carboniferous (316.1 ± 2.9 Ma)	19 / 15	5	0	21	47	26
This study, Tartèse et al. (2011a)	LRT-10	Lizio	2	MPG	Upper Carboniferous (316.4 ± 5.6 Ma)	29 / 18	0	3	59	28	10
Tartèse et al. (2011a)	LRT-15				Upper Carboniferous (319 ± 15 Ma)						
This study	HUEL-3	Huelgoat	1	MPG	Upper Carboniferous (314.0 ± 2.8 Ma)	18 / 0	6	0	50	17	28

Table 1: summary of zircon U-Pb data. Pop. = population.